END
DATE
FILMED
5-82
DTIC

MORPHODYNAMICS OF A MACROTIDAL BEACH:

BROOME, WESTERN AUSTRALIA.

L.D.WRIGHT , P.NIELSEN , A.D.SHORT and M.O.GREEN

DTIC
SELECTE
MAY 3 1982
D
H

Abstract

An intensive field investigation of hydrodynamic processes, processes of sediment entrainment and suspension, and morphologic change was carried out on an unprotected macrotidal beach near Broome in Northwestern Australia. The spring tide range was 9.5 metres; waves had heights of 0.5 to 1.2 metres and periods of 9 to 13 seconds. The beach had an overall concave upward profile with low gradient and dissipative subtidal and low-tidal zones, and steeper more reflective mid-tidal and high-tidal zones. Direct measurement of energy flux dissipation over the intertidal profile showed dissipation rates on the order of 2 to 5 watts per square metre of bed and indicated an approximate balance between shoaling and dissipation of unbroken waves so as to maintain a constant wave height. Time-averaged predictive estimates of wave work over the lunar half cycle for different points on the intertidal profile show similar dissipation rates and reveal a relatively uniform distribution of work over most of the profile but with maxima in the middle of the low-tidal zone and over the lower part of the high-tidal zone. Most of the work over the low-tidal and mid-tidal zones was performed by unbroken shoaling waves rather than by surf zone processes; surf zone processes only dominate over the high-tidal zone. The nature

of the surf zone processes varied across the profile as local gradient and degree of reflectivity changed with changing tide level. The growth of standing waves and infragravity ("surf beat") oscillations, as identified from spectra and cross spectra of surface elevation, η , and currents, u and v , was inhibited over most of the profile. However, well developed secondary standing wave energy, particularly at infragravity frequencies, was observed over the high-tidal zone at spring high tide and over the mid-tidal zone at neap high tide. Over the low-tidal and subtidal zones, strong shore-parallel tidal currents were subordinate only to the orbital velocities of unbroken incident waves. Over the subtidal zone asymmetrical tidal currents, skewed toward the north, attained maximum speeds of 0.5 m sec^{-1} just after high water. Field measurements of suspended sediment concentration profiles under broken and unbroken waves showed very good fit to a diffusion model for wave-induced sediment suspension and suggested that sediment suspension was probably attributable largely to waves. Northerly advection of wave-suspended sediment by asymmetrical tidal currents over the subtidal and low-tidal zones accounted for a net northerly longshore transport. The greatest morphologic mobility of the intertidal profile occurred over the lower high-tidal and upper mid-tidal zones corresponding to the position of the coarsest material and secondary maximum of time averaged wave work and to a beach state intermediate between the reflective and dissipative extremes. Temporally, the greatest mobility of the profile as a whole was observed on the short, within-tidal-cycle time scale. Net changes over the longest time scale of a lunar half cycle were negligible.

Introduction

Tidal effects on beach processes have received comparatively little attention in the literature despite the fact that a significant proportion of the world's beaches are situated in mesotidal or macrotidal environments. Prominent examples of studies which have examined beach morphologic changes over tidal cycles and between neap and spring tides include those by Strahler (1966), King and Barnes (1964), Watts and Dearduff (1954), and Gresswell (1937). The macrotidal beaches which occur around much of Great Britain have been particularly instructive in providing models of a geomorphological nature (e.g. King and Barnes, 1964; Gresswell, 1937). However, even though there have been several important hydrodynamic experiments carried out on beaches which experience high tidal ranges (e.g. Huntley and Bowen, 1975 a&b), the majority of these experiments have focused largely on non-tidal phenomena (waves, runup, etc.) rather than on the specific roles played by the tides in controlling beach dynamics. Macrotidal estuarine flats (e.g. Coleman and Wright, 1978; Semeniuk, 1981; Thom, et al., 1975) and tidal current processes over inner continental shelves (e.g. Seymour, 1980) have received considerably more attention.

Recent studies in Australia have demonstrated that microtidal beaches and surf zones may be dissipative, reflective, or in any of several intermediate states depending on local environmental conditions and on antecedent wave conditions (Wright, et al., 1979 a&b; Short, 1979 a&b). Modes of beach cut, amplitudes and frequencies of standing waves and possible edge waves, and relative strengths and scales of rip and longshore currents are strongly related to beach state (Wright, 1981; in press; Wright, et al., 1981). Depending on beach state, near bottom currents show variations in the relative dominance of motions due to: incident waves, subharmonic oscillations, infragravity

oscillations, and mean longshore and rip currents. Beach morphologic mobility and rate of change are similarly related to environmental conditions and associated modal (or most prevalent) beach state (Short, 1981; Short and Wright, 1981). Conditions of either persistently high wave energy or abundant fine grained sediment results in maintaining highly dissipative states which exhibit very low mobility. Such beaches are comparatively insensitive to erosion. The greatest degree of mobility is associated with the intermediate states.

In macrotidal environments, beach morphodynamic states may be expected to change with the tidal water level, η_t , with the result that the upper part of the profile may be morphodynamically different from the lower part. The relative roles played by different sediment-transporting phenomena such as progressive incident waves, standing waves and surf beats, and tidal currents should vary correspondingly across the beach as should beach mobility. In addition to their direct role in transporting sediment by means of tidal currents, high tidal amplitudes act together with wave processes by displacing the position of the surf zone. Consequently, any given point on the intertidal profile may be alternately dry, in the surf zone, and seaward of the surf zone. This paper reports the results of a series of field experiments conducted on a macrotidal beach near Broome in Northwestern Australia. The aims of these experiments were to assess the morphodynamic variability of the subtidal and intertidal beach/nearshore zones in relation to varying tidal levels and to determine the relative roles played by different nearshore and surf zone processes over different regions of the profile.

Experiment Site and Methods

The experiments were conducted on Cable Beach, near Broome, Western Australia (Fig. 1), over the period 11-30 November 1980. The beach is 16 km
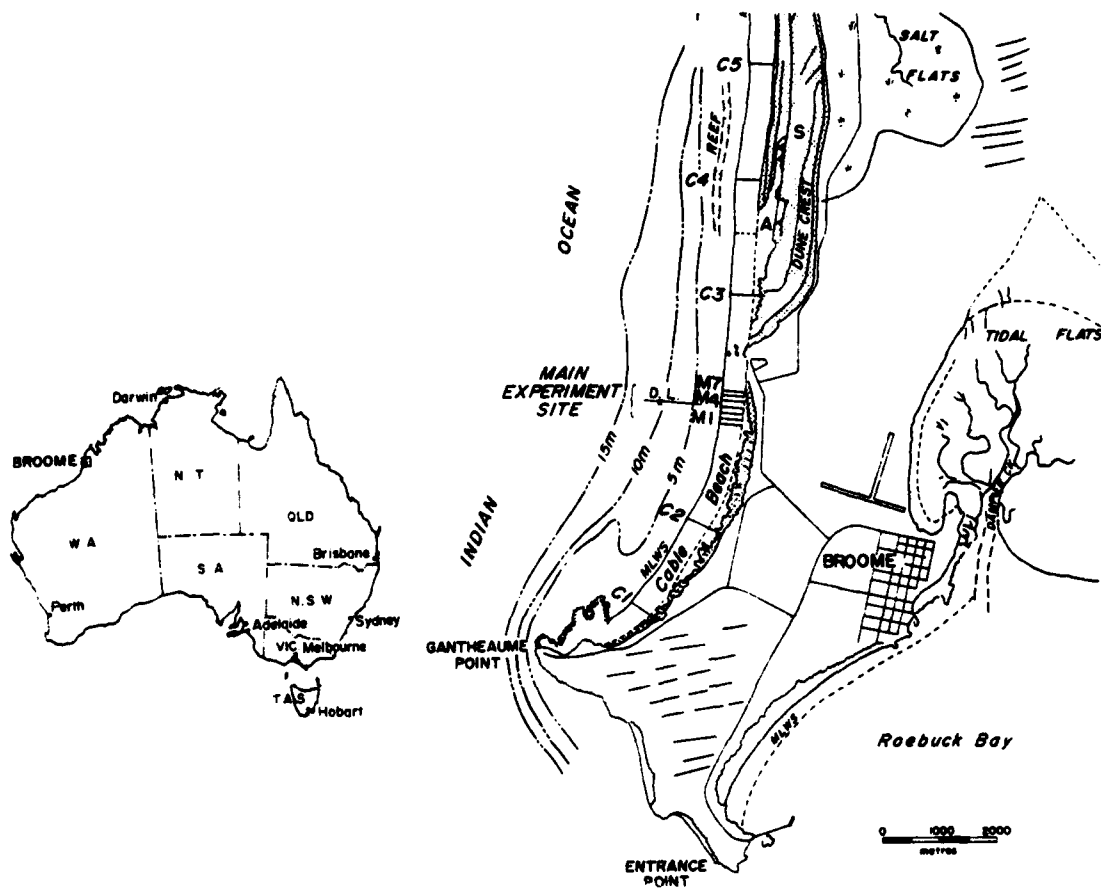
Figure 1. Location map of the study site. The main experiment site was centered on profile M-4. The location of the self-contained underwater data logging/current metering system is indicated by the initials D.L.

long and trends generally north-south facing the Indian Ocean. The main experiment site was situated 5 km north of the southern end of the beach and encompassed the survey lines labelled M1-M7 as shown in Figure 1. The site was chosen to avoid interference from the beach-rock reefs which lie offshore along much of the coast of this region. The beach is composed of typically fine but polymodal sand (~2.8ϕ; 0.135 mm) consisting of 60-75 percent $CaCo_3$ and 25-40 percent quartz. At the time of our observations, the beach had an average slope, tan β , of about 0.02; the intertidal beach was 350-400 metres wide. For a detailed description of the environment and estuarine tidal flat geomorphology of nearby King Sound, the reader is referred to Semeniuk (1981).

The region is under the influence of a tropical monsoon climate characterized by a winter (May to October) dry season and a summer (November to April) wet season. Offshore southeasterly winds dominate during the winter months generally maintaining calm seas and low wave energy. Most of the important wave energy arrives in association with the onshore winds of the summer season. Under normal summer conditions, moderate energy wind waves superimpose their effects on long period, low steepness westerly swell. During our experiment, wave heights ranged from 0.50 to 1.2 metres; peak periods were 9 to 13 seconds. Long-term wave statistics for the region are lacking.

An extreme tidal range is the most conspicuous feature of the environment of the study region. The tides are semidiurnal with a large neap-to-spring variation. The average spring tide range is 8.2 metres; the maximum range is 11 metres and the average neap range is only 1.8 metres. During the experiment period, the neap range was 2.0 metres and the spring range was 9.5 metres. The tide curve for Broome during the experiment period (11-30 November 1980) is shown in Figure 2. The time and duration of specific experiment runs are also indicated.
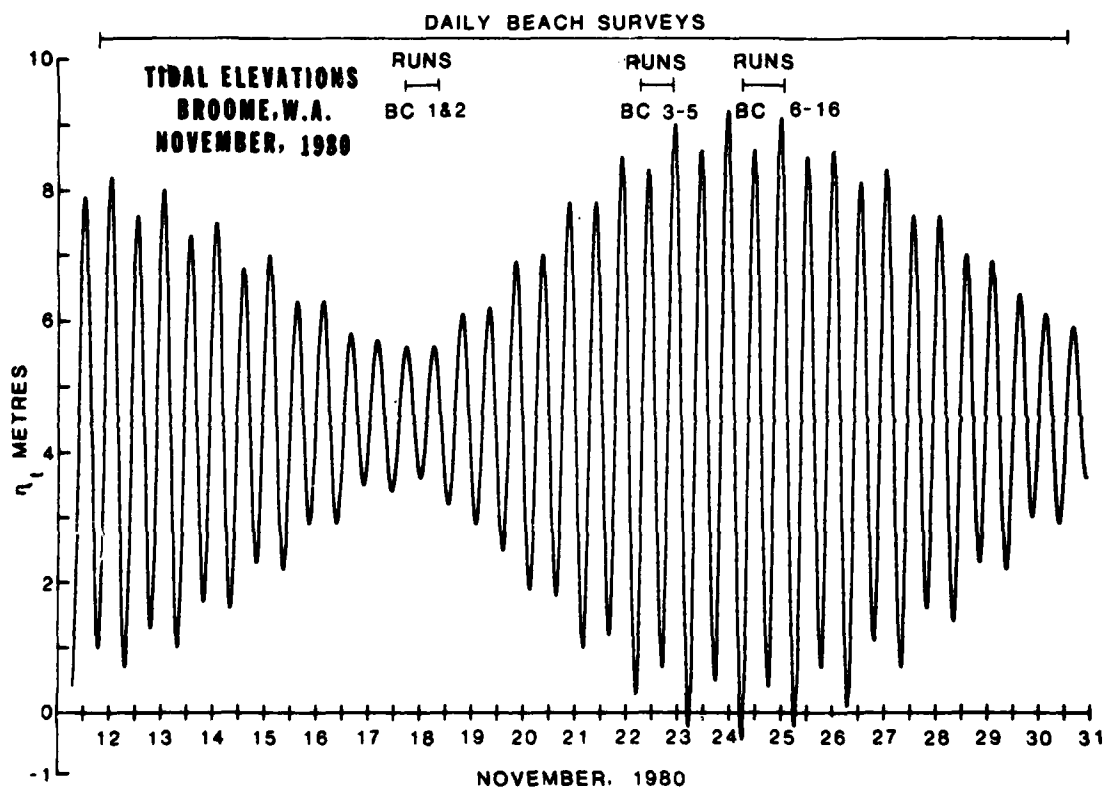
Figure 2.   Tidal elevations at Broome over the study period, 11-31 November 1980.
The zero position corresponds to mean spring low water. The horizontal
bars indicate the times and durations of experimental runs.

To determine morphologic characteristics and beach mobility, seven survey transects were established at 100 metre intervals along the beach, centered on the main experiment line (M4; Fig. 1) and were resurveyed on a daily basis throughout the study period. Seven additional transects along Cable Beach at 2 km intervals were surveyed once and confirmed that the profiles at the experiment site were generally representative of the beach as a whole. Subtidal and offshore zones were profiled using a Raytheon Model DE 719 surveying fathometer mounted on a small boat which was positioned by theodolite from shore. In addition to the day-to-day sand level changes as determined from surveys, maximum depths of disturbance occurring between consecutive surveys (i.e. within each tidal cycle) were estimated each day by means of plugs of colored sand placed in the beach alongside survey stakes.

Observations of flow velocity and pressure time series from the intertidal beach were made using the instrumentation system described by Bradshaw, et al. (1978). Strain gage pressure transducers and orthogonally mounted duct-impeller flow meters (Sonu, et al., 1974) were used respectively to measure pressure and currents (u, v). Sensors were sampled simultaneously at 1 second intervals and data were corrected for frequency-response characteristics (Nielsen and Cowell, 1981). Current (u, v) measurements from the subtidal zone (h = -8 m below MWL) were obtained by quasi-continuous burst recording using orthogonally mounted flow meters interfaced to an underwater data logger (indicated in Fig. 1). The interval between bursts was 6 minutes; a 100 second electronic filter was used to eliminate wave effects. A total of 15 separate experimental runs were made on the intertidal beach encompassing both neap and spring tide phases. Run lengths varied from 30 to 70 minutes. Figure 3 shows instrument locations for the different runs.
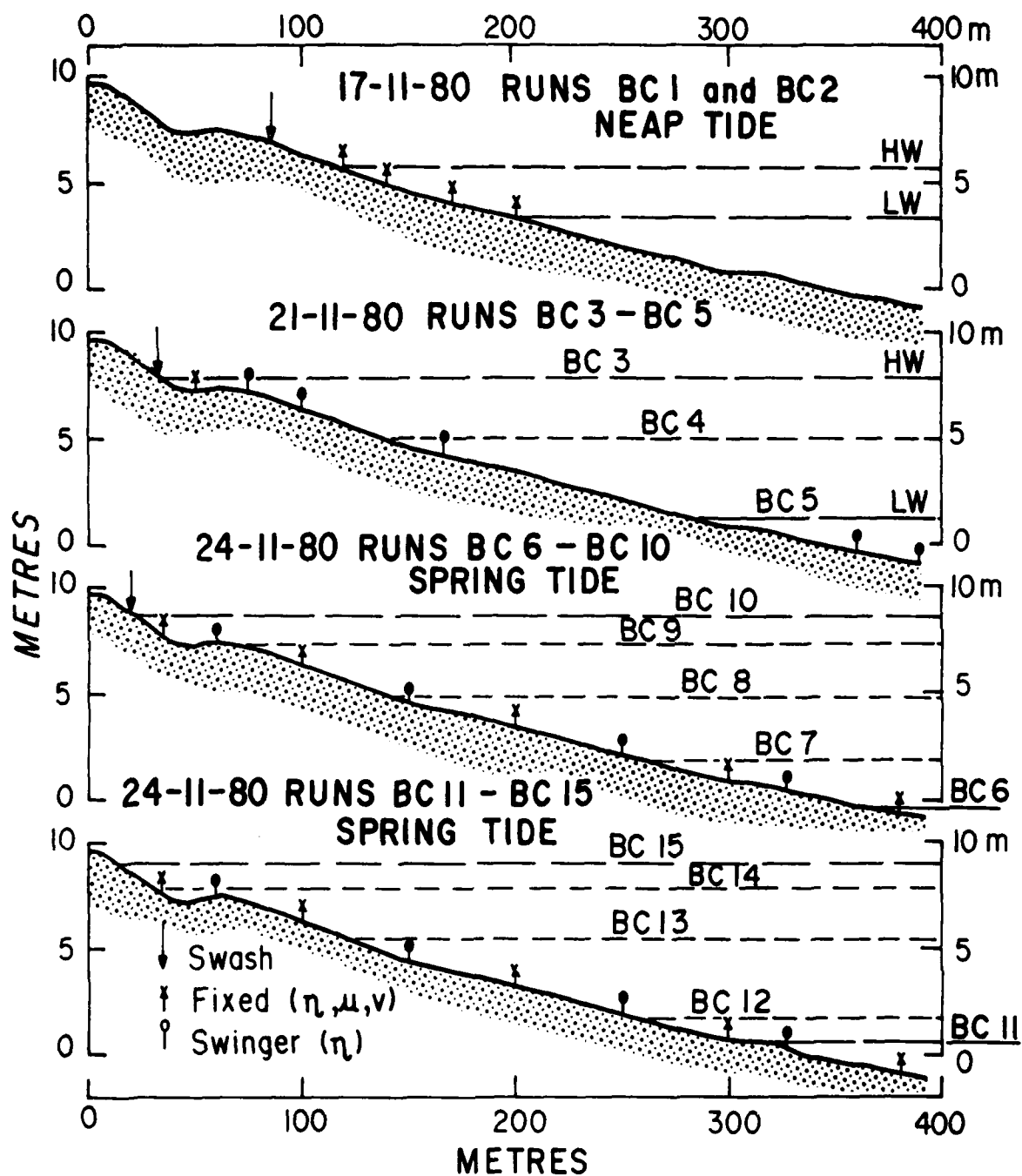
Figure 3. Instrument locations and tidal levels associated with different experimental runs.

Spectral and cross-spectral analyses were carried out on time series of η , u , and v from the intertidal beach using a fast Fourier transform. Spectral estimates were initially computed for 2 degrees of freedom; smoothing and increased degrees of freedom were accomplished by merging adjacent spectral estimates. Amplitudes of water surface oscillations (η) and horizontal current oscillations (u, v) in the incident wave (2 sec < T < 30 sec) and infragravity (T > 30 sec) frequency bands were estimated from the cumulative variance over those bands. A phase relationship of 90° $(\pi/2)$ between η and u at any given frequency was used as a test for the existence of standing waves at that frequency. Additional current statistics including net mean $(\bar{u}, \bar{v})$, root mean squared (u_{rms}, v_{rms}) and root mean cubed velocities were computed for the two horizontal flow components. The resulting wave and current statistics for different runs and intertidal positions are presented in Table 1.

Profiles of suspended sediment concentration under breaking and non-breaking waves were measured in a series of 22 shorter runs under different wave conditions. The suction sediment sampler described by Nielsen and Green (in press) was used. The device permits simultaneous sampling from 7 levels above the bed by way of thin intake tubes which create minimal disturbance to flow. Concentrations can be measured to within 1 centimetre of the bed.

Morphologic Characteristics and Tidal Zonation

Longshore uniformity was a general characteristic of Cable Beach in the vicinity of the experiment site throughout the experiment period. Except for the ephemeral appearance and disappearance of beach cusps on the extreme upper limits of the high tidal beach, rhythmic or aperiodic longshore irregularities such as crescentic bars, transverse bars, or rip channels were typically absent. The morphology is thus well described in terms of the cross-sectional profile.

TABLE 1

OBSERVED WAVE AND CURRENT STATISTICS OVER THE

INTERTIDAL BEACH, CABLE BEACH, BROOME, W.A. NOVEMBER 1980

INTERTIDAL ZONE	Run	x (m)	h_x (m)	H_s (m)	u_s (m s⁻¹)	H_{in} (m)	u_{in} (m s⁻¹)	v_{in} (m s⁻¹)	$\bar{u}$ (m s⁻¹)	$\bar{v}$ (m s⁻¹)	u_{rms} (m s⁻¹)	v_{rms} (m s⁻¹)	$(\bar{u}^3)^{1/3}$ (m s⁻¹)	$(\bar{v}^3)^{1/3}$ (m s⁻¹)	T_p secs
LOW-TIDAL ZONE	BC 5	390	1.7	0.24	0.38	0.04	0.054	0.055	-0.08	-0.21	0.214	0.22	-0.174	-0.23	11.4
	BC 5	360	1.1	0.25	0.45	0.05	0.085	0.06	-0.014	-0.24	0.23	0.26	+0.19	-0.26	11.4
	BC 6	380	0.5	0.25	0.51	0.07	0.21	0.16	-0.65	-0.25	0.284	0.28	-0.225	-0.30	12.8
	BC 7	380	2.9	0.26	0.26	0.03	0.05	0.04	-0.001	-0.26	0.134	0.26	+0.055	-0.264	12.7
	BC 7	327	1.6	0.25	-	0.08	-	-	-	-	-	-	-	-	12.7
	BC 7	300	1.0	0.32	-	0.05	-	-	-	-	-	-	-	-	12.7
	BC 8	380	5.6	0.27	0.20	0.03	0.04	0.06	-0.027	-0.109	0.104	0.119	-0.10	-0.127	12.0
	BC 8	300	3.6	0.31	-	0.04	-	-	-	-	-	-	-	-	12.0
	BC 8	250	2.5	0.29	-	0.09	-	-	-	-	-	-	-	-	12.0
	BC 8	200	1.5	0.30	0.43	0.05	0.065	0.06	-0.029	-0.124	0.22	0.14	-0.10	-0.15	12.0
	BC 9	380	8.3	0.28	0.15	0.022	0.06	0.08	-0.071	-0.056	0.11	0.079	-0.123	-0...	12.8
	BC 9	300	6.4	0.30	-	0.03	-	-	-	-	-	-	-	-	12.8
	BC 9	200	4.3	0.28	0.25	0.03	0.03	0.03	-0.038	-0.054	0.133	0.072	-0.117	-0.081	12.8
	BC10	380	9.2	0.32	-	0.032	-	-	-	-	-	-	-	-	12.5
	BC10	300	7.3	0.36	-	0.032	-	-	-	-	-	-	-	-	12.5
	BC10	200	5.2	0.34	0.27	0.04	0.035	0.075	-0.052	+0.236	0.15	0.244	-0.14	+0.251	12.5
	BC12	380	2.5	0.37	-	0.037	-	-	-	-	-	-	-	-	12.0
	BC12	300	0.8	0.43	-	0.07	-	-	-	-	-	-	-	-	12.0
	BC13	380	6.2	0.26	-	0.03	-	-	-	-	-	-	-	-	11.3
	BC13	300	4.36	0.30	-	0.03	-	-	-	-	-	-	-	-	11.3
	BC13	200	2.56	0.30	0.38	0.04	0.05	0.04	-0.018	-0.114	0.195	0.13	-0.111	-0.14	11.3
	BC14	380	8.55	0.34	-	0.06	-	-	-	-	-	-	-	-	12.0
	BC14	300	6.81	0.38	-	0.045	-	-	-	-	-	-	-	-	12.0
	BC14	200	5.01	0.35	0.29	0.048	0.035	-	-0.031	-	0.15	-	-0.122	-	12.0
	BC15	380	9.2	0.30	-	0.028	-	-	-	-	-	-	-	-	11.1
	BC15	300	7.4	0.32	-	0.029	-	-	-	-	-	-	-	-	11.1
	BC15	200	5.7	0.30	0.23	0.03	0.027	-	-0.057	-	0.131	-	-0.137	-	11.1
	BC16	380	9.6	0.32	-	0.03	-	-	-	-	-	-	-	-	12.5
	BC16	300	7.9	0.34	-	0.036	-	-	-	-	-	-	-	-	12.5
	BC16	200	6.1	0.31	0.26	0.033	0.08	0.085	-0.052	+0.201	0.138	0.213	-0.134	+0.22	12.5
MID-TIDAL ZONE	BC 1	200	2.0	0.41	0.44	0.04	0.046	0.05	-0.057	-0.03	0.23	0.081	-0.196	-0.082	13.0
	BC 1	170	1.5	0.38	0.55	0.12	0.07	-	+0.026	-	0.28	-	-0.07	-	13.0
	BC 1	140	0.5	0.38	0.65	0.07	0.20	0.05	-0.20	+0.007	0.4	0.038	-0.41	+0.063	13.0
	BC 1	120	0.3	0.10	0.33	0.04	0.39	-	+0.032	-	0.186	-	+0.34	-	13.0
	BC 2	200	0.2	0.46	0.50	0.06	0.06	0.05	-0.076	-0.046	0.25	-	-0.23	-	11.4
	BC 2	170	1.5	0.42	0.53	0.09	0.11	-	+0.044	-0.051	0.29	0.051	+0.15	-0.051	11.4
	BC 2	140	0.5	0.40	0.70	0.09	0.19	0.025	-0.14	+0.002	0.37	0.022	-0.35	+0.041	11.4
	BC 2	120	0.25	0.07	0.65	0.05	0.22	-	+0.16	-	0.37	-	+0.5	-	11.4
	BC 9	150	3.0	0.32	-	0.08	-	-	-	-	-	-	-	-	12.8
	BC 9	100	1.4	-	0.61	-	0.095	-	-0.019	-	0.309	-	+0.159	-	12.8
HIGH-TIDAL ZONE	BC 3	100	1.6	0.41	0.5	0.084	0.10	0.07	-0.057	+0.085	0.26	0.12	-0.22	+0.133	10.7
	BC 3	75	0.75	0.36	0.85	0.11	0.22	0.15	-0.122	+0.074	0.46	0.15	-0.45	+0.165	10.7
	BC 3	50	0.67	0.26	0.45	0.045	0.30	0.14	-0.25	+0.10	0.36	0.15	-0.40	+0.17	10.7
	BC10	100	2.4	-	0.55	-	0.07	-	-0.015	-	0.275	-	+0.135	-	12.5
	BC10	60	1.0	0.29	-	0.11	-	-	-	-	-	-	-	-	12.5
	BC10	35	1.0	0.18	0.50	0.11	0.13	-	-0.10	-	0.29	-	-0.31	-	12.5
	BC14	100	1.81	0.34	0.65	0.11	0.26	-	-0.12	-	0.37	-	-0.34	-	12.0
	BC14	35	0.51	0.30	-	0.12	-	-	-	-	-	-	-	-	12.0
	BC15	100	2.40	-	0.65	-	0.17	-	-0.053	-	0.34	-	-0.25	-	11.1
	BC15	35	1.1	0.30	-	0.08	-	-	-	-	-	-	-	-	11.1
	BC16	100	2.9	-	0.65	-	0.18	-	-0.023	-	0.36	-	-0.17	-	12.5
	BC16	35	1.6	0.32	0.43	0.09	0.16	-	-0.114	-	0.25	-	-0.24	-	12.5

x = distance seaward; h_x = depth; H_s = significant wave height; u_s = orbital velocity of significant waves;
u_{in}, v_{in} = shore-normal and shore parallel components of bottom velocity due to infragravity oscillations;
$\bar{u}$, $\bar{v}$ = net, time averaged shore normal and shore parallel current speeds; u_{rms}, v_{rms} = root-mean-squared
values of u and v; $(\bar{u}^3)^{1/3}$, $(\bar{v}^3)^{1/3}$ = root mean cubed values of u and v; T_p = peak wave period; u values are
positive in onshore direction; v values are positive for flows toward the north. Each value presented has
been computed from 2,000 to 4,000 data points measured at 1 second intervals over periods varying from
30 to 70 minutes.

Overall, the profile extending from the backshore seaward to about -10 metres below spring low water has a pronounced concave upward shape as shown in Figure 4. A moderately wide (~350 m) intertidal zone lying between the high and low spring tide limits separates a backshore capped by a high (~18 m) foredune from a wide and very low gradient subtidal zone. The subtidal zone which lies below the level of spring low water and is permanently subaqueous has the lowest gradient (tan β = .009 - .011) and is composed of the finest sediment (mean grain size < 0.1 mm or ~3ϕ). The surface of the subtidal zone was capped by small, symmetrical wave-induced ripples throughout the study period.

The profile morphology of the intertidal beach is illustrated in more detail in Figure 5. The intertidal beach can be subdivided into 3 zones, each of which is distinguished by different morphologic and sediment characteristics, frequencies of inundation, and dynamic regimes. The low-tidal zone extends from the level of spring low tide to the level of neap low tide. The mid-tidal zone is centered on the position of mean sea level and extends from neap low tide to neap high tide; and the high-tidal zone extends from neap high tide to spring high tide. The tidal levels shown in Figure 5 are those which prevailed during the study period rather than the annual means.

The upper curve in Figure 5 indicates the fraction of time (or probability) that any given point on the profile is inundated by the tide over the lunar half cycle (that is, over the fortnightly neap-to-neap or spring-to-spring cycle). The curve expresses the probability (or fraction of total time), $p \{\eta_t \geq Z_b\}$, that any given tidal elevation, η_t equals or exceeds any given intertidal bed elevation, Z_b , estimated from

$$p \{\eta_t > Z_b\} \simeq \cos^2 \left(\frac{\pi}{2} \frac{Z_b - \eta_{min}}{\eta_{max} - \eta_{min}}\right) \qquad (1)$$
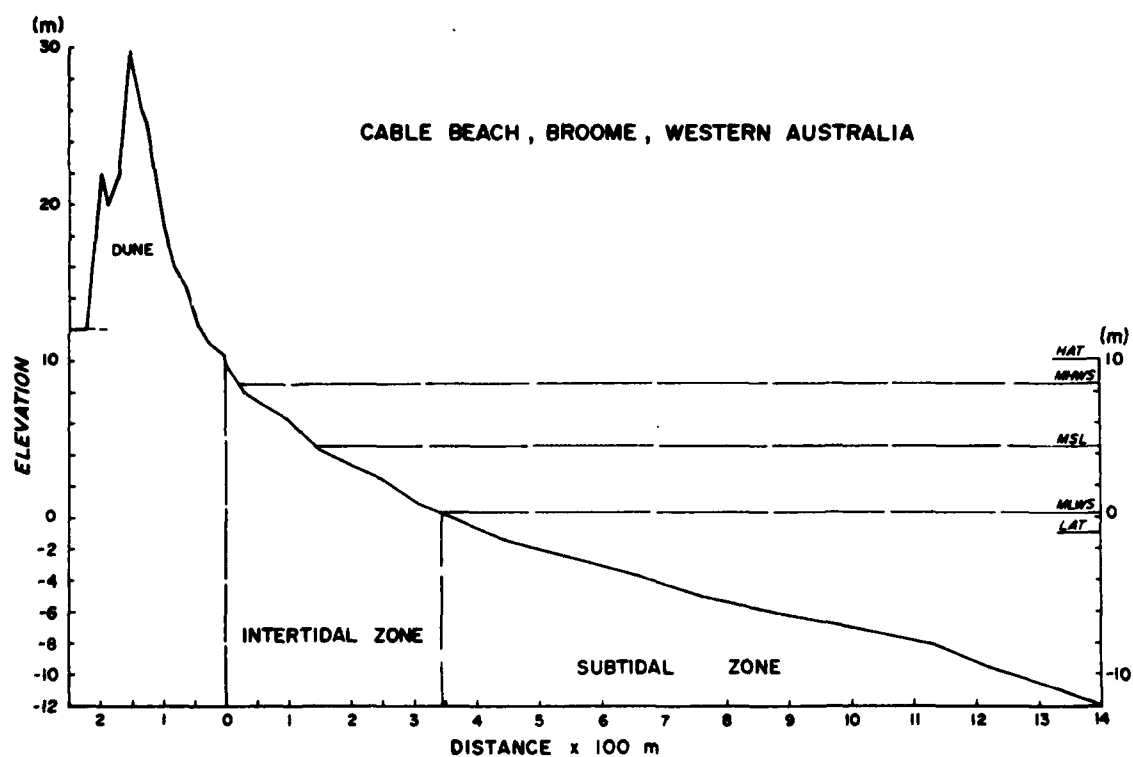
Figure 4. General profile of the subtidal, intertidal, and backshore zones of Cable Beach (profile M-4; based on survey of 12-14 November 1980).
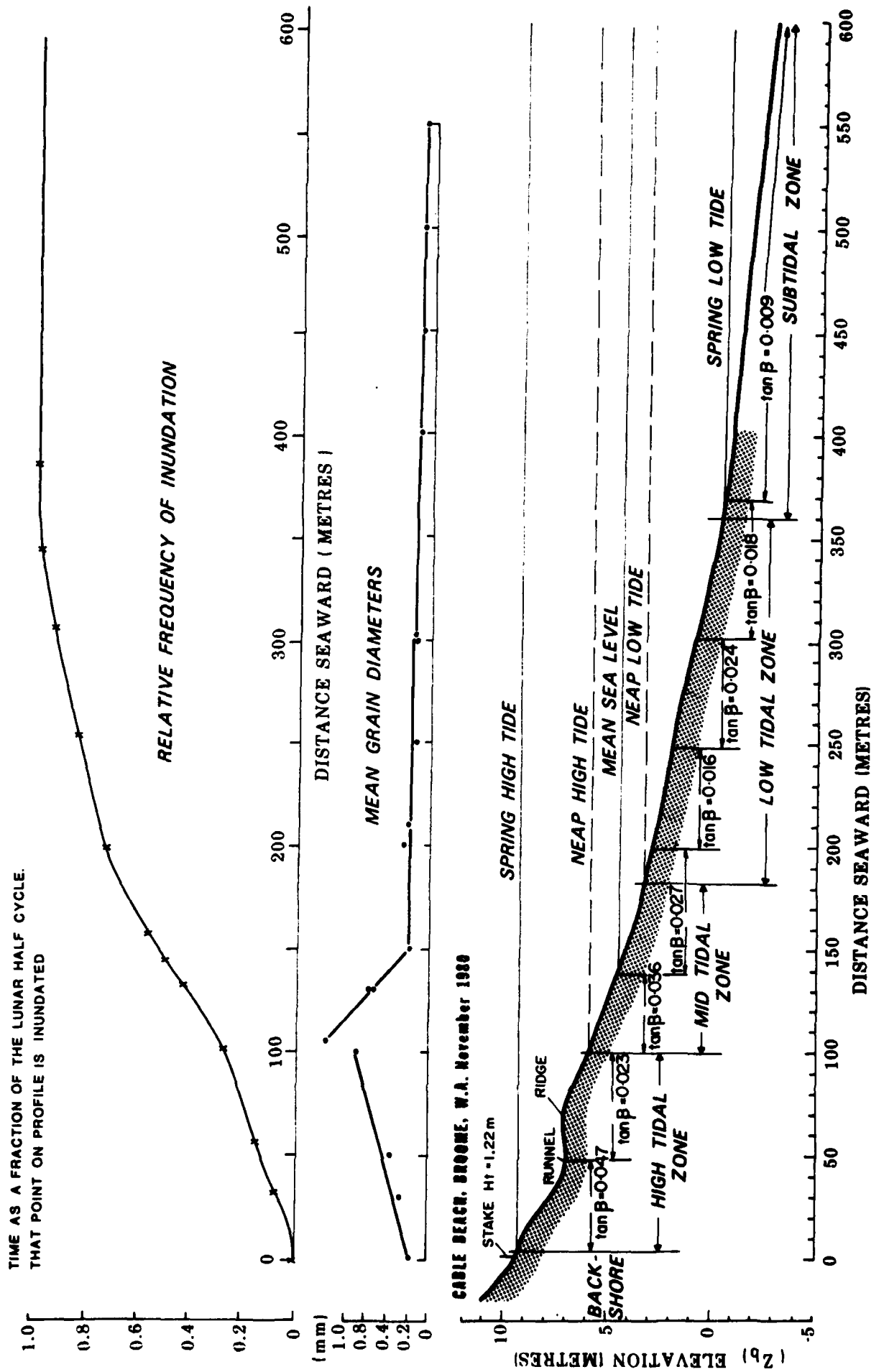
TIME AS A FRACTION OF THE LUNAR HALF CYCLE.
THAT POINT ON PROFILE IS INUNDATED

RELATIVE FREQUENCY OF INUNDATION

DISTANCE SEAWARD (METRES)

MEAN GRAIN DIAMETERS

CABLE BEACH, BROOME, W.A. November 1980

STAKE Ht = 1.22 m

RIDGE
RUNNEL

BACK-
SHORE

tanβ = 0·047
tanβ = 0·023

HIGH TIDAL
ZONE

tanβ = 0·056
tanβ = 0·027

MID TIDAL
ZONE

tanβ = 0·016
tanβ = 0·024

LOW TIDAL ZONE

tanβ = 0·018
tanβ = 0·009

SUBTIDAL ZONE

SPRING HIGH TIDE
NEAP HIGH TIDE
MEAN SEA LEVEL
NEAP LOW TIDE
SPRING LOW TIDE

DISTANCE SEAWARD (METRES)

ELEVATION (METRES) (z_b)

Figure 5. Morphologic details of the subtidal and intertidal profiles, definitions of intertidal zones, variation in grain diameter, and relative frequency of inundation over the profile (profile M-4).

- 14 -

where η_{max} and η_{min} are respectively the maximum and minimum tidal elevation (η_t) levels. From the curve it can be seen that the low tidal zone is inundated for about 72 percent of the time or more, depending on the exact elevation of any point; the lower and upper limits of the mid-tidal zone are respectively inundated for 72% and 25% of the time, and the high tidal zone is reached by the tide for less than 25% of the time.

The middle curve in Figure 5 shows the observed mean sand sizes across the profile. The coarsest material (mean grain diameter ~1 mm) occurred near the upper limit of the mid-tidal zone. Seaward of this position, sediments exhibited a progressive fining.

The low-tidal zone was the widest of the three intertidal zones owing to the low gradient. The lower portion of this zone was continuous with and very similar to the subtidal zone. Except for a very subtle "ridge" or "hump" in the region around x = 260 metres (Z_b = 1.5 - 2.0 m ; Fig. 5), the low tidal zone was essentially featureless. The mid-tidal zone exhibited a steeper gradient and was generally smoother, lacking wave-generated ripples. The greatest relief and steepest slopes prevailed in the high-tidal zone. A steep uppermost beach face, active only during spring high tides, was fronted by a relatively pronounced runnel which separated it from a ridge about 1 metre high and composed of the coarsest sand. Although this ridge occupied the high-tidal zone, it was also within the neap high tide swash zone of the mid-tidal zone and had the characteristics of a berm. The runnel had a rippled surface related to longshore drainage. The multiple ridges and runnels described by King (1972), Davis, et al. (1972) and others were generally absent from Cable Beach except for this single ridge and runnel system on the high-tidal zone.

Observed Rates of Dissipation of Wave Energy Over the Intertidal Beach

As waves propagate shoreward across the intertidal profile into water of decreasing depth, they experience shoaling, refraction, and dissipation. Since on Cable Beach the waves were almost entirely normally incident, and longshore variations in topography were trivial, the refraction effects can reasonably be ignored. Acting alone, shoaling in the shallow waters close to shore would cause a shoreward increase in wave height while conserving energy flux. However, where there is dissipation, energy flux diminishes shorewards and the effects of shoaling on changing wave heights are reduced or reversed. Wave energy dissipation is a fundamental nearshore process: it bears heavily on gradients in radiation stress and hence on nearshore circulation; it determines the amount of energy flux which eventually reaches the active beach; and it is directly equivalent to the rate at which the waves perform work. The mechanisms responsible for energy dissipation include turbulence and internal friction, bed friction, and the interaction of waves with currents including tidal currents. Although turbulent dissipation is dominant in surf zones, bed friction is probably most important seaward of the break point. Dissipation by bed friction has particular morphodynamic significance, since it is equivalent to the work done in entraining and transporting sediments.

Energy flux, P , is

$$P = E C_g \tag{2}$$

where E is energy density and C_g is group velocity. The energy density, E , is related to observed significant wave height (Table 1) by

$$E = \frac{1}{16} \rho g H_s^2 \tag{3}$$

- 16 -

where ρ is water density, g is acceleration of gravity, and H_s is significant wave height as estimated from the total variance in the wind wave and swell band. Since all observations over the intertidal profile were made in relatively shallow water with respect to the long (> 10 secs) peak period, we assume linear shallow water waves and estimate C_g from

$$C_g = C = \sqrt{g h} \qquad (4)$$

where C is phase speed and h is local instantaneous depth. This assumption is not strictly valid for estimates of C_g over the low-tidal zone at high tide; however, it introduces no more error than would result from a monochromatic wave assumption.

The dissipation rate, expressed in units of watts per unit area of bed surface is

$$\frac{dP}{dx} = \frac{d}{dx} \left(\frac{1}{16} \rho g H_s^2 \sqrt{g h} \right) \qquad (5)$$

From the direct simultaneous observations of H_s and h, at different points on the profile (Table 1), it is possible to estimate the average dissipation rate over the interval, Δx , separating any two consecutive stations from

$$\frac{\Delta P}{\Delta x} = \frac{1}{16} \rho g^{3/2} \frac{\left[H_{s(1)}^2 h_{(1)}^{1/2} \right] - \left[H_{s(2)}^2 h_{(2)}^{1/2} \right]}{\Delta x} \qquad (6)$$

where the subscripts (1) and (2) respectively denote the values at the deeper and shallower stations.

The dissipation rate, dP/dx is related to wave-induced bed shear stress τ and instantaneous bottom velocity maxima by

$$\frac{dP}{dx} = \tau \, u_s = \frac{2}{3\pi} \rho \, f \, u_s^3 \tag{7}$$

(Jonsson, 1967) where f is a dimensionless friction or dissipation factor. Since we are able to estimate dP/dx , we can assess the associated values of a dissipation coefficient f_e from

$$f_e = \frac{\Delta P}{\Delta x} / \frac{2}{3\pi} \rho \, u_s^3 \tag{8}$$

Values of f_e estimated in this way include all dissipative effects, not just bed friction alone. The corresponding coefficient, f_w , for bed friction only can be predicted as function of the ratio of bottom orbital semi-excursion a_s (= u_s/ω , where ω is the wave radian frequency) to roughness length, k , from

$$f_w = \exp\left[5.213\left(\frac{a_s}{k}\right)^{-.194} - 5.977\right] \tag{9}$$

for situations where $a_s/k > 1.7$ or

$$f_w = 0.28 \qquad \text{when } a_s/k \leq 1.7 \tag{10}$$

(Swart, 1974). The roughness length k , can be estimated from

$$k = 120 \, d + 1.2 \, \eta_r \tag{11}$$

where d is grain diameter and η_r is ripple height (Nielsen, 1981; in press). Methods for predicting η_r for cases where it is not known can be found in Nielsen (1981).

Table 2 gives values of P_1 , energy flux at the deeper of any two stat.ɔɔ points, the dissipation rates, $\Delta P/\Delta x$, the estimated values of f_e and the predicted values of f_w for smooth (η_r = 0) and rippled beds based on local grain sizes. Mean values for each of the three intertidal zones are given in Table 3.

TABLE 2

Observed dissipation rates, dissipation factors,
and bottom friction factors

Intertidal Zone	Run	x₁(m)	x₂(m)	h₁(m)	h₂(m)	P_1 watts m⁻¹	$\frac{\Delta P}{\Delta x}$ watts m⁻²	f_e	f_w smooth	f_w rippled
Low Tidal Zone	BC 7	380	327	2.9	1.6	228	1.34	0.37	0.051	0.076
	BC 8	300	250	3.6	2.5	360	1.94	0.44	0.045	0.064
	BC 8	250	200	2.5	1.5	262	0.9	0.08	0.048	0.062
	BC 9	300	200	6.4	4.3	448	1.28	0.572	0.057	0.131
	BC 10	300	200	7.3	5.2	690	1.7	0.59	0.052	0.106
	BC 12	380	300	2.5	0.8	428	1.24	0.024	0.045	0.08
	BC 13	300	200	4.4	2.6	370	1.86	0.212	0.055	0.125
	BC 14	300	200	6.8	5.0	742	2.08	0.52	0.057	0.130
	BC 15	300	200	7.4	5.7	550	1.28	0.64	0.045	0.115
	BC 16	300	200	7.9	6.1	622	1.54	0.56	0.057	0.130
Mid-tidal Zone	BC 1	200	170	2.0	1.5	470	4.00	1.46	0.047	0.050
	BC 1	170	140	1.5	0.5	350	4.92	1.02	0.041	0.041
	BC 2	200	170	2.0	1.5	590	5.48	0.184	0.04	0.046
	BC 2	170	140	1.5	0.5	426	6.24	0.128	0.039	0.039
	BC 2	140	120	0.5	0.25	224	11.00	0.169	0.051	0.054
	BC 10	200	60	5.2	1.00	520	2.52	0.204	0.055	0.077
	BC 14	200	100	5.0	1.8	540	2.26	0.238	0.048	0.070
	BC 15	200	100	5.7	2.4	424	1.08	0.036	0.045	0.080
High Tidal Zone	BC 3	100	75	1.6	0.75	920	7.92	0.424	0.072	0.112
	BC 3	75	50	0.75	0.66	222	4.5	0.642	0.068	0.157
	BC 10	60	35	1.0	1.0	166	4.00	0.168	0.055	0.069
	BC 14	100	35	1.8	0.5	308	1.80	0.048	0.05	0.065
	BC 15	100	35	2.4	1.1	294	1.92	0.048	0.05	0.065
	BC 16	100	35	2.9	1.6	302	1.28	0.120	0.055	0.07

P_1 = energy flux at x_1, h_1; $\frac{\Delta P}{\Delta x}$ = rate of energy flux dissipation; f_e = observed dissipation factor; f_w(smooth) = estimated bottom friction factor for unrippled bed; f_w (rippled) = estimated bottom friction factor for observed (local) ripple characteristics.

* these values are unusually low, may be suspect.

TABLE 3

Mean dissipation rates and mean dissipation and
friction factors for Cable Beach

Intertidal zone	$\left(\overline{\dfrac{\Delta P}{\Delta x}}\right)$ watts m^{-1}	$\left(\overline{\dfrac{\Delta P}{P_1 \Delta x}}\right)$ % m^{-1}	$\overline{f_e}$	$\overline{f_w}$ smooth	$\overline{f_w}$ rippled	$\dfrac{\overline{f_e}}{\overline{f_w}}$ (rippled)
Low tidal	1.42	0.33	0.400	0.051	0.102	3.92
Mid-tidal	4.76	1.35	0.150	0.046	0.057	2.64
High tidal	2.58	1.33	0.242	0.058	0.090	2.66

Values for dissipation rates expressed as percentages of total energy flux dissipated per metre are also indicated in Table 3. Several important features are evident from Tables 2 and 3. In terms of absolute dissipation rates, the lowest values occurred in association with the generally greater depths and smaller roughness lengths of the low-tidal zone. The highest were observed in the mid-tidal zone. Typical values for the comparatively low wave conditions under which the experiments were conducted (Table 1) were on the order of 2 to 5 watts per square metre for unbroken waves. An inspection of the H_s values in Table 1 suggests that although dissipation caused significant shoreward decreases in P , H_s and hence E experienced little variation between consecutive stations in any given run. This suggests an approximate balance between the effects of shoaling and dissipation and it can be inferred that shore-normal gradients in radiation stress outside the narrow, migrating surf zone were negligible.

The dissipation factor, f_e , was significantly larger than the predicted bed friction factor, f_w , for smooth or rippled beds. This suggests that only part of the total dissipation was due to bed friction. Since only three of the data points listed in Table 2 were in the vicinity of the surf zone, it must be inferred that most of the excess dissipation (above that expected for bed friction alone) was probably due to internal turbulence and wave-current interaction. It must be noted that non-linear changes in C_g may also have been operative (R.T. Guza, Personal Communication). The greatest excess (as expressed by the ratio f_e/f_w) occurred over the low-tidal zone where f_e was four times as large as f_w (estimated for rippled bed conditions) suggesting that bed friction accounted for only about 25 percent of the total dissipation in that region. Notably, net time-averaged current velocities, especially longshore tidal current velocities, were significantly higher over the low-tidal and subtidal zones and it is likely that these currents were the source of the excess dissipation.

Predictions of Frictional Dissipation Rates and Work Distribution Over a Lunar Half Cycle

The dissipation rates just described were observed at discrete times and for discrete tidal elevations. Although they convey information about relative dissipation rates over different zones and about f_e and f_w , they are insufficient to support more quantitative arguments concerning the time-averaged dissipation rates and work distribution. From a morphodynamic viewpoint, it is valuable to know the average rate of work expended by the waves on the bed over a complete lunar half cycle. In this context, we are concerned not so much with rates of wave decay as with the amount of dissipation arising specifically from bed friction. Since friction dissipation rates vary with water depth, considerable variation over a tidal cycle can be expected for any given point on the profile. Furthermore, since the surf zone is continually migrating back and forth across the intertidal profile, part of the total work is performed by unbroken waves and part is related to surf zone processes. We can predict these effects.

To begin, we must consider dissipation which takes place over the subtidal zone prior to breaking at different levels of the tide since this will determine the wave heights and energy fluxes which actually reach the intertidal region. The total dissipation ΔP over the subtidal profile, from h_∞ the depth at the outer subtidal zone limits (approximately "deep water") to h_o the depth at the inner subtidal zone limit where the intertidal zone begins is simply the integral of the dissipation over the subtidal interval $h_o - h_\infty$ (or $x_o - x_\infty$) or in other words

$$\Delta P = \int_{h_\infty}^{h_o} \frac{dP}{dx}\ dx = \int_{h_\infty}^{h_o} \frac{2}{3\pi}\ \rho\ f_w\ u_{max}^3\ dx = \frac{1}{8}\ \rho\ g\ (H_\infty^2\ C_{g_\infty} - H_o^2\ C_{g_o}) \qquad (12)$$

where subscripts $_\infty$ and $_o$ denote respectively outer and inner values. Since h_∞ and h_o vary with tidal elevation, η_t , ΔP will also vary over a tidal cycle

assuming the interval is held constant. Figure 6 shows the predicted energy flux loss over the subtidal zone expressed as fraction of energy flux, P_∞ , at the outer limit, plotted for different tidal levels, η_t . The values shown are for wave heights H_∞ of 1 and 2 metres and a wave period of 11 seconds; the observed subtidal gradient of $\tan \beta = .009$ and width of 10.5 km were used. The diagram indicates only slight subtidal dissipation at high tide; at low tide energy flux is reduced by about 50%. Predicted changes in wave height are very small, how-ever, since shoaling roughly balances frictional dissipation. This simply means that the height, H_o of waves entering the intertidal zone can be considered roughly the same as H_∞ (except along beach sections fronted by subtidal beach-rock reefs).

The time-averaged total dissipation rate by bed friction, $(dP/dx)_t$ and its distribution across the intertidal profile is probably fundamental to molding the morphology of the intertidal beach since it is equivalent to the rate of doing work. To estimate $(dP/dx)_t$ for any given elevation Z_b on the intertidal profile, it is necessary to consider the local roughness conditions and the associated average friction factor, f_w , as well as the probability distribution of time-varying depths, $h(Z_b , \eta_t)$ over the different points on the profile. To understand the modes of dissipation, it is also necessary to separate the contributions to total dissipation by surf zone processes $(dP/dx)_s$, versus that associated with non-breaking waves (nearshore processes) $(dP/dx)_n$.

The total average dissipation rate is thus

$$(\frac{dP}{dx})_t = (\frac{dP}{dx})_s + (\frac{dP}{dx})_n = \int_{tidal\ cycle} \frac{dP}{dx} (H_o , \eta_t)\ p(\eta_t)\ d\eta_t \qquad (13)$$
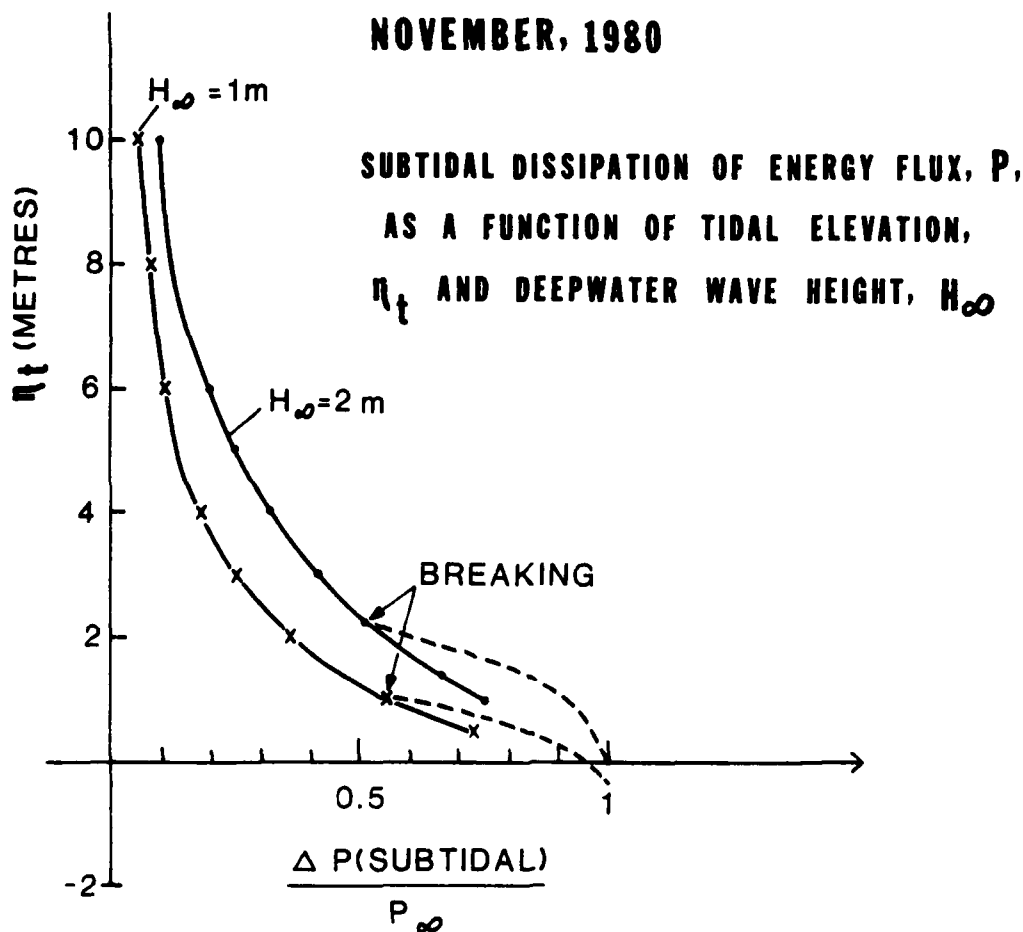
surf   non-
zone   breaking

Figure 6. Subtidal dissipation of energy flux, P , as a function of tidal
elevation, η_t , and deep water wave height, H_∞ . The loss of energy
flux, ΔP , is expressed as a fraction of the total deep water energy
flux, P_γ .

where $p(\eta_t)$ is the probability density of any given tidal elevation, η_t

$$p(\eta_t) = \frac{\pi}{2(\eta_{max} - \eta_{min})} \; \sin \left(\pi \frac{\eta_t - \eta_{min}}{\eta_{max} - \eta_{min}} \right) \qquad (14)$$

More explicitly, assuming shallow-water waves,

$$\left(\frac{dP}{dx}\right)_t = \frac{1}{12\pi} \, \rho \, f_w \, g^{3/2} \left[\gamma^3 \int_{\eta_t = z_b}^{\eta_t = z_b + H_o/\gamma} h^{3/2}_{(\eta_t, z_b)} \; p(\eta_t) \;\; + \int_{\eta_t = z_b + H_o/\gamma}^{\eta_{max}} H_o^3 \, h^{-3/2}_{(\eta_t, z_b)} \; p(\eta_t) \right] (15)$$

$$\text{surf part} \qquad\qquad \text{non-breaking part}$$

where the local instantaneous depth $h = z_b - \eta_t$ and γ is the breaking ratio H/h which for Cable Beach was observed to have a value of about 0.75. Figure 7 shows the distribution of $(dP/dx)_t$ as computed from Equation 15 for a lunar half cycle using the tidal conditions of the study period and different wave heights. The friction factor, f_w , was varied locally in accordance with observed grain size and predicted roughnesses. The local values of f_w are indicated on the profile. Hypothetical dissipation rates for a smooth bed are also indicated. The curves indicate a work maximum roughly in the middle of the low-tidal zone and a secondary maximum over the lower part of the high-tidal zone. The latter is attributable to the coarser grain sizes and larger ripples of the high-tidal and upper mid-tidal zones; it is not present in the "smooth bed" estimates. The dissipation rates predicted for 0.5 metre waves correspond reasonably well with the rates observed for similar wave conditions (Tables 2 and 3). Figure 7 also suggests that for the small waves — which are the modal waves for Cable Beach — the work is distributed fairly uniformly across most of the intertidal beach. Cross-profile gradients in dissipation rate increase with increasing wave height.
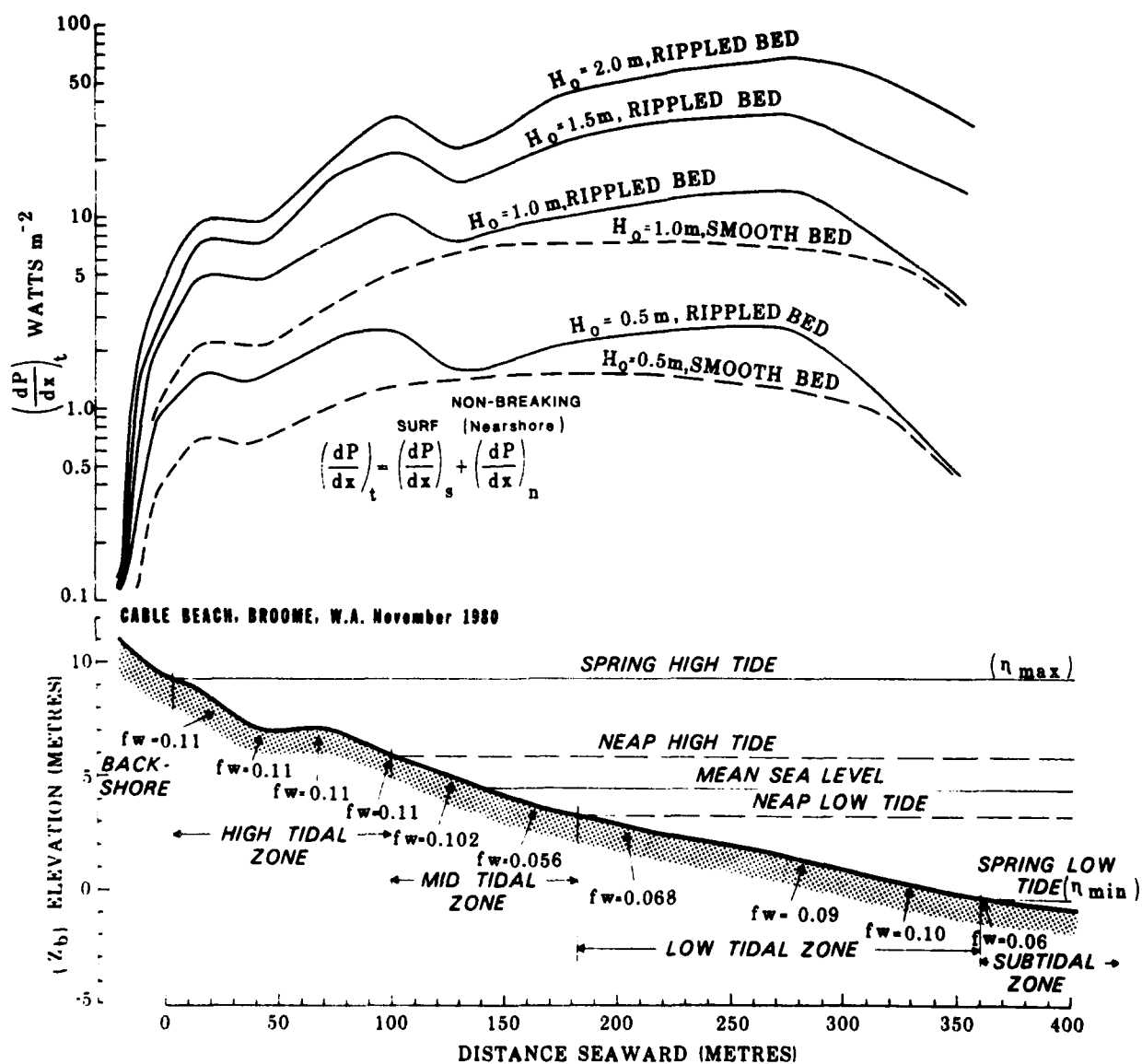
Figure 7. Average energy flux dissipation rates $(dP/dx)_t$ over the lunar half cycle as computed from equation 15 for different wave heights, H_0. The solid curves show the distribution computed on the basis of the actual local friction factors f_w for the rippled bed. The associated f_w values are indicated on the profile. The dashed curves show the hypothetical dissipation rates for a smooth, unrippled bed.

Figure 8 shows the proportion of the total dissipation, $(dP/dx)_t$, that is
accounted for by the surf zone part, $(dP/dx)_s$, for different wave heights. It
can be inferred that non-breaking wave processes are dominant when

$$(\frac{dP}{dx})_s \ / \ (\frac{dP}{dx})_t \ < \ 0.5$$

and surf zone processes are dominant when   .

$$(\frac{dP}{dx})_s \ / \ (\frac{dP}{dx})_t \ > \ 0.5$$

On this basis, Figure 8 indicates that even during the relatively rare occurrence
of 2 metre waves, the low-tidal zone is entirely dominated by non-breaking wave
processes suggesting that, dynamically, this zone is more analogous to a nearshore
zone of wave shoaling than it is to a beach. For lower energy conditions (e.g.
$H_o \leq$ 1 m), this is also true of the mid-tidal zone. Under the modal low wave-
height conditions, only the uppermost portion of the high-tidal zone is dominated
by surf-zone processes.

Surf-Zone Processes

Although surf zone processes only dominate the upper parts of the intertidal
profile, the continual sweep of the surf zone across the profile subjects every
intertidal point to surf zone processes at some stage in the lunar half cycle.
In a general sense, the same basic surf zone processes that operate on microtidal
beaches should be operative on macrotidal beaches. In particular, the breaking
process should be the same and the basic distinction between dissipative versus
reflective surf zone behavior should apply. In the majority of cases on Cable
Beach, breakers were transitional between plunging and spilling over the low-tidal
and mid-tidal zones and typically plunging over the ridge on the high-tidal zone.
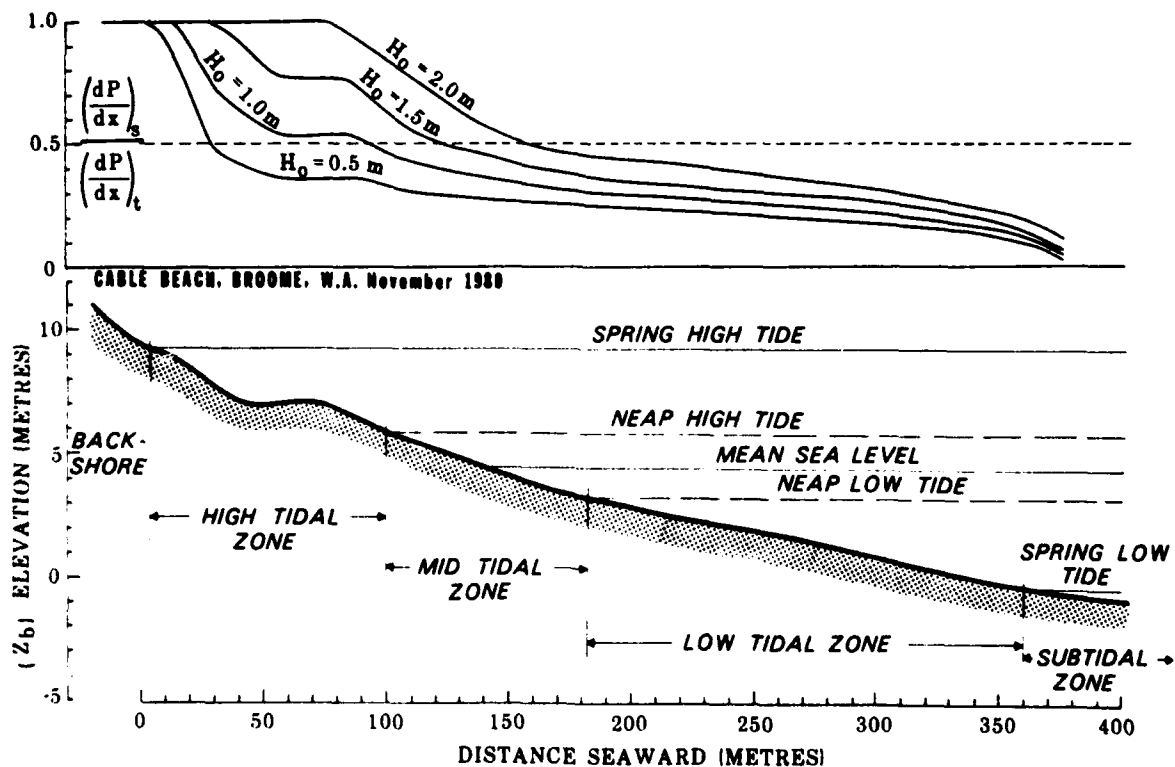
Figure 8.   Time-averaged (lunar half cycle) surf-zone dissipation rate $(dP/dx)_s$
            relative to the total (surf zone plus non-breaking) dissipation rate
            $(dP/dx)_t$.   When the curve lies below the 0.5 level, the implication
            is that more work is performed by non-breaking shoaling waves than
            by surf zone processes.

During high spring tides, surging breakers were observed on the extreme upper beach face for short periods. Reliable statistical evaluations of the ratio $\gamma = H_b/h$ (where H_b is breaker or bore height) were generally precluded by the non-stationarity of h due to changing tidal levels. However, rough estimates from individual breakers suggest that γ had a value of about 0.75 over most of the profile.

As the migrating breaker zone traverses different local bed gradients, the degrees of reflectivity or dissipativeness change. Dissipativeness or reflectivity can be indexed by the surf scaling parameter

$$\varepsilon = a_b \omega^2/g \, \tan^2 \beta \qquad (16)$$

where a_b is breaker amplitude, ω = radian frequency ($2\pi/T$) and β is local gradient (Guza and Inman, 1975; Wright, et al., 1979). Guza and Inman (1975) showed that low values of ε ($\varepsilon \simeq 1.0 - 2.5$) define reflective conditions conducive to the occurrence of standing wave motions at incident wave frequencies and particularly at subharmonic frequencies (one half incident wave frequency) in association with subharmonic edge waves which are most strongly developed under these conditions. At the opposite extreme, fully dissipative beaches and surf zones are characterized by ε values on the order of $10^2 - 10^3$. Figure 9 shows the variation of local values of ε across the intertidal beach computed for 12-second waves of different heights. The diagram indicates that, even for the low 0.5 m waves, the low-tidal zone is highly dissipative. The steeper upper beach face of the high-tidal zone is reflective with respect to 0.5 metre waves and moderately reflective with higher waves. When the waves experience partial dissipation and height reduction over the ridge and reform over the runnel, the upper beach face should be even more highly reflective.
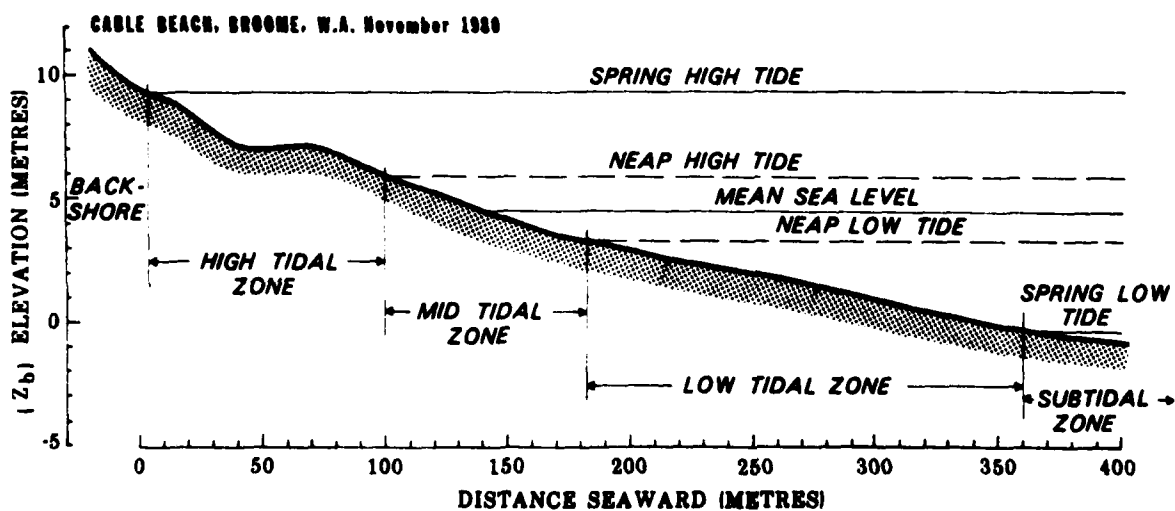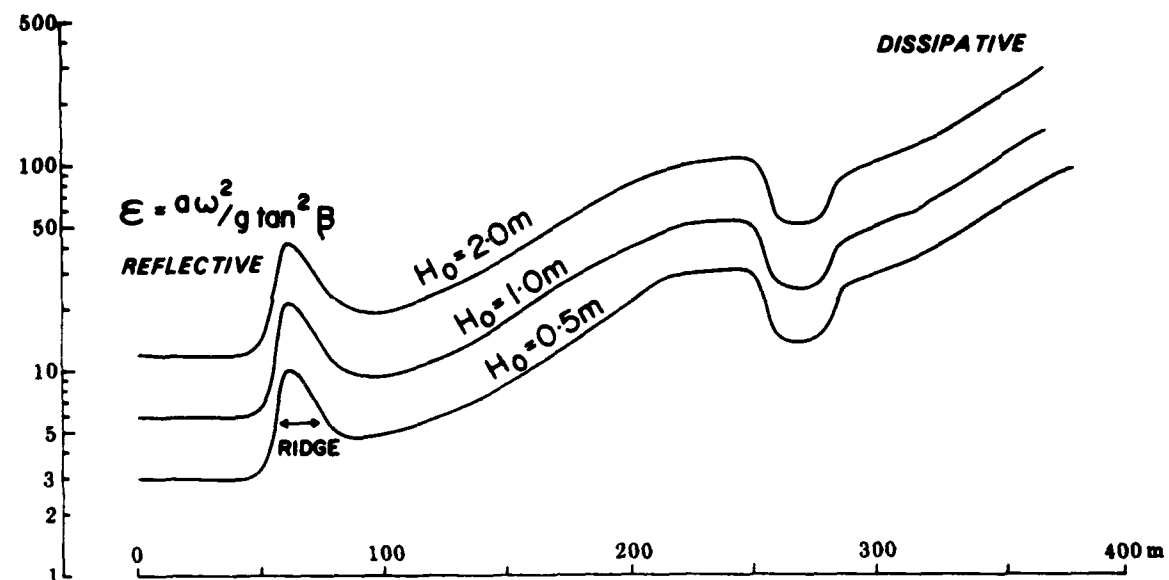
$$\varepsilon = a\omega^2 / g \tan^2 \beta$$

REFLECTIVE

DISSIPATIVE

$H_0 = 2.0m$

$H_0 = 1.0m$

$H_0 = 0.5m$

RIDGE

CABLE BEACH, BROOME, W.A. November 1980

SPRING HIGH TIDE

NEAP HIGH TIDE

MEAN SEA LEVEL

NEAP LOW TIDE

BACK-SHORE

HIGH TIDAL ZONE

MID TIDAL ZONE

LOW TIDAL ZONE

SPRING LOW TIDE

SUBTIDAL ZONE

(Z_b) ELEVATION (METRES)

DISTANCE SEAWARD (METRES)

Figure 9.   Variation across the intertidal profile of the surf-scaling parameter, ε , computed for 12-second incident waves of different heights.

Field observations from microtidal environments have shown that standing wave motions are present in reflective, dissipative, and intermediate surf zones and are probably important in molding the surf zone and beach morphologics (Wright, et al., 1979a; Wright, in press). Under reflective conditions, sub-harmonic edge waves are dominant (Wright, et al., 1979 a&b; Wright, in press); under dissipative conditions standing waves at infragravity or "surf beat" frequencies (periods of 30 to 300 seconds) prevail and may, in fact, dominate the spectrum in the inner surf zone (Wright, et al., 1981; Wright, in press). There is mounting evidence which suggests that at least a large fraction of surf beat energy has the form of edge waves (Fujinawa, 1979; Huntley, 1976; Huntley, et al., 1981; Holman, 1981). Since edge waves gain their maximum amplitudes through processes of resonant growth (e.g. Guza and Davis, 1974), a minimum "spin up" time of several cycles is implied for both subharmonic and surf beat oscillations. However, in macrotidal environments, where water depths and horizontal surf zone positions are continually changing, causing associated changes in surf zone gradient, β , it could be expected a priori that there may be insufficient time to permit resonant growth to the maximum possible amplitude.

During spring tides on Cable Beach, the absolute average rate of depth change over the period of one-half hour either side of mid tide would be roughly .068 cm sec^{-1} corresponding to a horizontal rate of change of position of 2.13 cm sec^{-1}. In one wave cycle the shoreline position would experience a horizontal displacement of about 25 cm or about 2 metres per typical "surf beat" cycle. Near high and low tides the rate of vertical change is less: the average rate of depth change during the half-hour periods before or after high or low tides is only .009 cm sec^{-1}. This would cause a horizontal surf zone migration rate of about 0.5 cm sec^{-1} over the low tide zone at low tide or 0.19 cm sec^{-1} over the high

tide profile at high tide. At neap tides, the mid tide, high tide, and low tide horizontal migration rates across the mid-tidal zone would be about 0.5 cm sec^{-1}; 0.06 cm sec^{-1}; and 0.08 cm sec^{-1} respectively. Intuitively, one would thus expect standing waves or edge waves to be best developed at neap tides over the mid-tidal zone and at spring high tides on the upper part of the high-tidal zone.

Spectra and cross spectra of water surface elevation, η , and horizontal current motion, u and v , reveal the presence of infragravity standing waves in most runs; however, as would be expected, the amplitudes of these oscillations were consistently low. Figure 10 shows typical intertidal spectra and cross spectra from the upper mid-tidal zone (x = 100 m) and from the high-tidal zone (x = 50 m) based on time series obtained just prior to peak spring tides. Infra-gravity peaks are present for η and u in both sets of spectra in the frequency band 0.01 hz to 0.02 hz (50-100 secs). Coherence between η and u is significant for the infragravity peaks; the associated phase relationships of 90° ($\pi/2$) between η and u indicate that the infragravity oscillations were standing in the shore-normal direction. The infragravity energy from the high-tidal zone was appreciably higher than that from the upper mid-tidal zone. The shore-normal velocity amplitude of the infragravity oscillations corresponding to the u peak in the high-tidal zone spectrum shown in Figure 10 was 30 cm sec^{-1} as compared to the incident wave maximum orbital velocity, u_s , of 45 cm sec^{-1} (Table 1). Similar high infragravity velocities appear in two sets of spectra from the neap tide surf zone over the mid-tidal zone. However, in all cases infragravity energy was subordinate to incident waves (Table 1). Such a situation contrasts markedly with that of microtidal dissipative or intermediate beaches (Wright, et al., 1981).
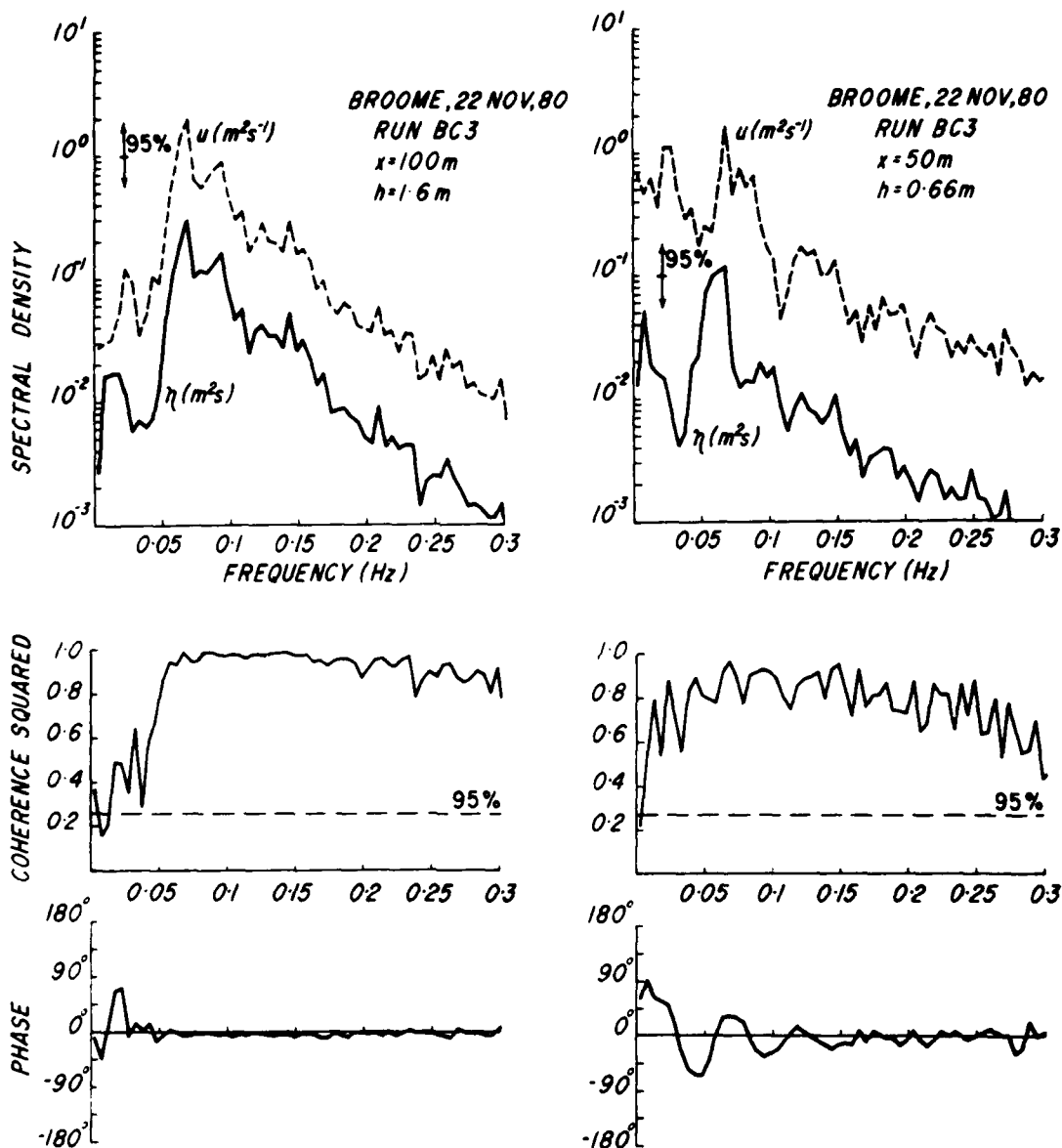
Figure 10.   Power spectra, coherence, and phase of surface elevation η (pressure) and shore normal current, u measured over the mid-tidal (x = 100 m) and high-tidal (x = 50 m) zones.

Tidal Currents and Other Currents

Tidal currents and other non-wave induced flows are second in importance to wave orbital velocities over the sub-tidal and low-tidal zones. Over the sub-tidal zone, strong reversing tidal currents paralleling the trend of the coast were observed during a continuous monitoring period. Figure 11 shows the time series of filtered (100 sec time constant) shore-parallel current velocities v_t, as recorded from $\bar{h}$ = -8 metres below mean sea level at 1 metre above the bed over the subtidal zone, together with the associated tidal water surface elevations, η_t. The semi-diurnal tidal periodicity in the current record is immediately apparent as is the approximate phase correspondence between v_t and η_t.

The most important feature of the record is the asymmetry of northerly versus southerly setting currents about the zero position. Northerly setting velocity maxima of 40 to 50 cm sec^{-1} occurred within 1 hour after high water. Southerly flows of shorter duration attained their maxima of only 20 to 25 cm sec^{-1} about 1 hour after low tide. As a consequence of this asymmetry, a net time averaged residual current velocity of 12.7 cm sec^{-1} set toward the north (computed over an integer number of 5 cycles). This asymmetry may be due to nearshore topographic effects: a possible analog could be the well-known mutual evasion of flood-and-ebb channels in estuaries (e.g. Price, 1963). By implication one would anticipate a region of southerly dominated transport to exist farther offshore.

Other features of the current record (Fig. 11) include a more rapid absolute acceleration rate under rising tide than during falling tide and the superimposition of velocity fluctuations corresponding approximately to a one-hour cycle. The acceleration asymmetry, manifest in Figure 11 as a rapid increase in speed just prior to the northerly (high tide) maxima followed by a more gradual rate of decrease in speed following the maxima, reflects the
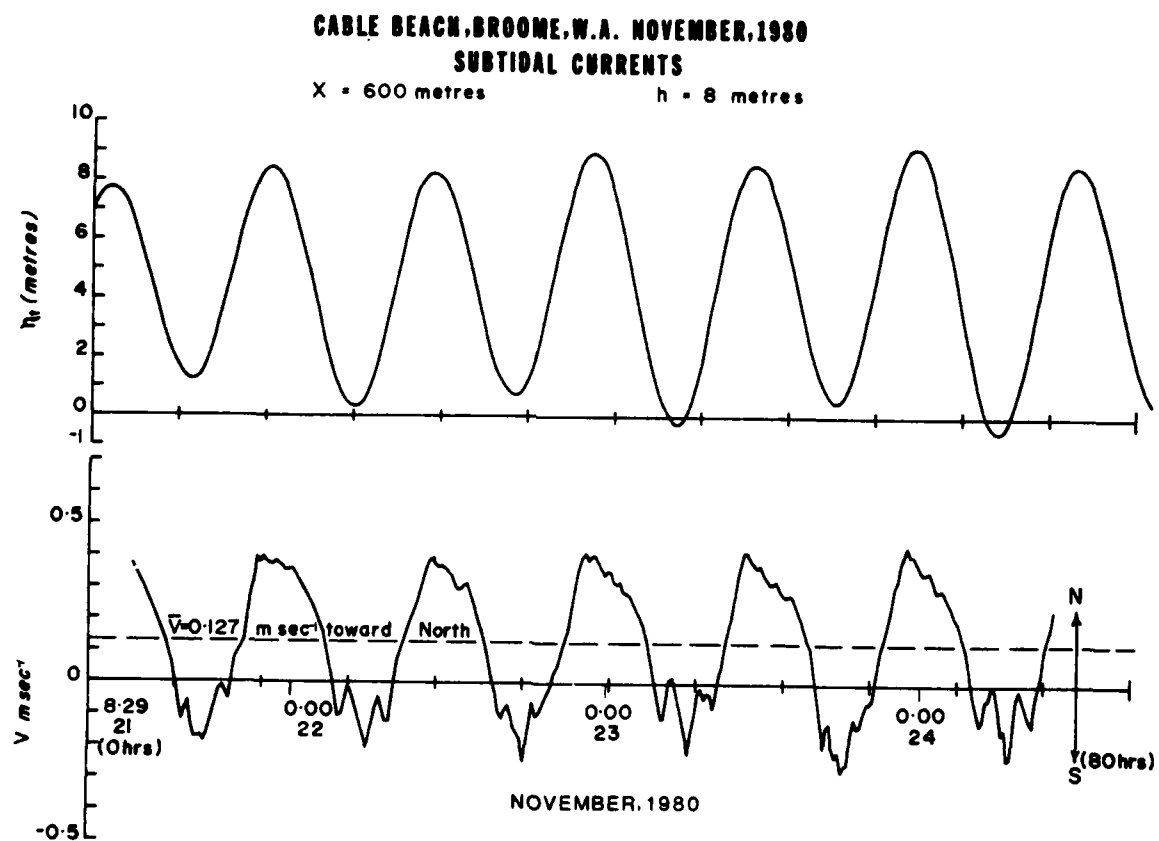
Figure 11. Shore-parallel current velocity, v , as recorded over the subtidal
zone from a depth of -8 metres below mean water level and corre-
sponding tidal elevations, η_t .

contribution of the first (~6 hours) and higher harmonics of the semidiurnal oscillation and is a common feature of tides in shallow water and estuaries (e.g. Pingree and Griffiths, 1979; Boon and Byrne, 1981). The subordinate oscillations at about 1 hour are most obvious in the southerly-setting "trough"; however, they appear to be present as more subtle features throughout the record. This is possibly a topographic effect.

From Table 1, it is seen that time averaged $\bar{v}$ components (averaged over experimental runs) were also relatively strong over the low-tidal zone and attained speeds of up to 25 cm sec^{-1} in both northerly and southerly directions. However, $\bar{v}$ values were very much lower (on the order of 5 cm sec^{-1}) over the mid-tidal and high-tidal zones and a comparison of the v_{in} and $\bar{v}$ columns in Table 1 suggests that over those zones surf beat contributed more to longshore flows than did tides. Net shore-normal flows, $\bar{u}$, near the bed were typically weak with speeds of less than 10 cm sec^{-1} in most cases. Most of these flows were seaward-directed and were probably return flows compensating shoreward transports near the surface (e.g. Wright, et al., 1981).

Figure 12 shows a graphic comparison of the average relative speeds of wave orbital velocities, u_s , infragravity oscillations, u_{in} and v_{in} , net shore normal flows, $\bar{u}$, and shore parallel currents due mainly to tides, v_t over the subtidal zone and each of the intertidal zones. The values on the bars of the histograms are all expressed as proportions of the local average value of u_s (which is shown as 1.0 for comparison). Wave effects were dominant over all zones. However, shore parallel tidal currents were nearly as swift as u_s over the subtidal zone and played significant secondary roles over the low-tidal zone; they decrease dramatically over the mid-tidal and high-tidal zones. A shoreward growth in average strength of infragravity oscillations accompanied the shoreward slackening of v_t .
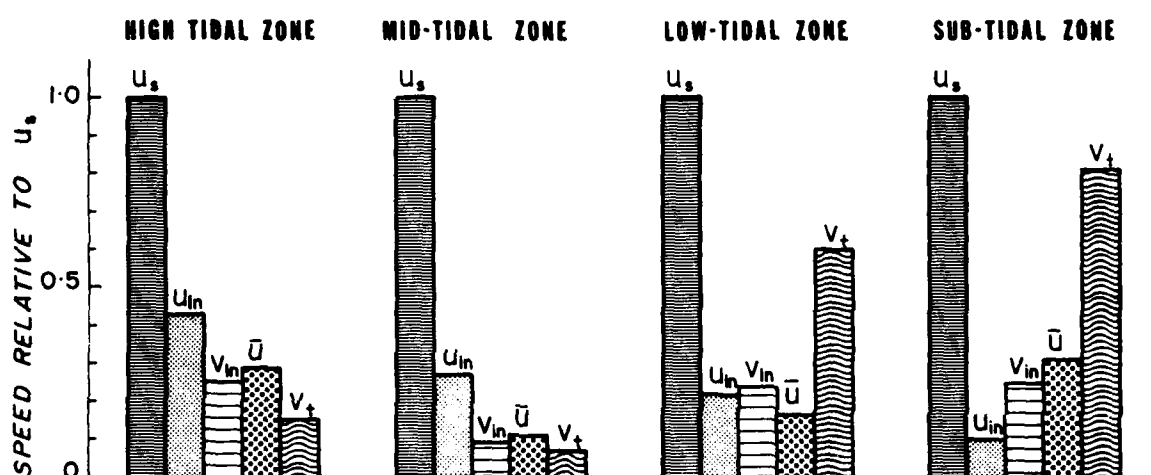
HIGH TIDAL ZONE   MID-TIDAL ZONE   LOW-TIDAL ZONE   SUB-TIDAL ZONE

SPEED RELATIVE TO u_s

1·0

0·5

0

u_s u_{in} v_{in} $\bar{u}$ v_t

u_s u_{in} v_{in} $\bar{u}$ v_t

u_s u_{in} v_{in} $\bar{u}$ v_t

u_s u_{in} v_{in} $\bar{u}$ v_t

Figure 12.   Relative speeds of significant wave orbital velocities, u_s, infra-gravity oscillations u_{in} and v_{in}, net shore normal flows, $\bar{u}$, and shore parallel tidal currents, v_t, over the subtidal, low-tidal, mid-tidal, and high-tidal zones. Values are all shown as non-dimensional ratios of the local average values of u_s which are assigned values of 1.

- 37 -

Sediment Suspension and Transport

No direct measurements of net sediment transport were made on Cable Beach; however, from the foregoing, some important inferences concerning sediment transporting processes can be drawn: (1) Wave-induced oscillatory flows, u_s , dominate over other modes of flow everywhere over the subtidal and intertidal regions (Fig. 12) so one would expect waves to play the dominant role in entraining and suspending sediment. (2) Over most of the beach more work is performed by unbroken waves, usually acting on a rippled bed than by surf zone processes (Fig. 8). Field and laboratory evidence (Nielsen, 1979; Nielsen and Green, in press) indicates that seaward of the surf zone, phase-dependent sediment suspension by wave-induced vortices dominates over wave-induced bedload transport. (3) Owing to the pronounced asymmetry of non-wave currents, particularly the shore-parallel tidal currents (Fig. 11), significant net longshore advection of sediment at least over the subtidal and low-tidal zones is implied. Most of this probably involves advection of sediment initially placed in suspension by waves although some direct bed load transport by the currents themselves probably occurs.

The total sediment transport rate, Q_t , consists of a suspended load component Q_s and a bed load component Q_b . Although several investigators have concluded that in surf zones suspended load transport is small relative to bed load (e.g. Komar, 1978), those researchers considered sediment transport in intermittent suspension within 10 centimetres of the bed to be part of the bed load. Our measurement and analysis procedures permit all transport which involves grain support by fluid forces (as opposed to grain-to-grain support) to be analyzed as suspended load (Nielsen and Green, in press). It is clear that seaward of surf zone, suspended transport is dominant. The suspended load transport rate, Q_s , is

$$Q_s = \int_0^h \overline{U}(z) \, \overline{C}(z) \, dz \tag{17}$$

where $\overline{U}(z)$ and $\overline{C}(z)$ are respectively the mean velocity and mean sediment concentration at z elevation above the bed. For the Cable Beach case, current data suggest that suspended sediment concentrations, $\overline{C}(z)$ should be dominated by wave motion. To test this, the results of the 22 measured concentration profiles (described in the methods section) were fitted to the diffusivity model for wave induced sediment transport described by Nielsen (1979) and Nielsen and Green (in press).

The measured concentration profile points $\overline{C}(z)$ were fitted to a curve of the general form

$$\overline{C}(z) = C_o \exp \left\{ - \frac{\overline{w}h}{\sqrt{E_b E_s}} \tan^{-1} \frac{\sqrt{E_s}}{E_b} \left(\frac{z}{h}\right) \right\} \tag{18}$$

or for unbroken waves, the simple exponential form

$$\overline{C}(z) = C_o \exp \left(- \frac{\overline{w}}{E_b} z\right) \tag{19}$$

where C_o is the concentration at the bed, $\overline{w}$ is average settling velocity of the sediment, E_b is the near bed diffusivity and E_s is the diffusivity associated with turbulence generated outside the bottom boundary layer (Nielsen and Green, in press). Equations 18 and 19 follow the diffusion model

$$\overline{C}\,\overline{w} + E \frac{d\overline{c}}{dz} = 0 \; , \quad E = E_b + E_s \left(\frac{z}{h}\right)^2 \tag{20}$$

The extrapolated bed concentration, C_o , is a function of the skin friction shields parameter Θ'

$$\Theta^{'} = \frac{1/2 \, f_w \, \rho \, u_s^2}{(\rho_s - \rho) \, g \, d} = \frac{1/2 \, f_w \, \rho \, (a_s w)^2}{(\rho_s - \rho) \, g \, d} \tag{21}$$

where ρ_s is sediment density, d is grain diameter and a_s is orbital semi-excursion near the bed. Bed diffusity, E_b , was shown by Nielsen and Green (in press) to be a function of the ratio $u_s/\bar{w}$, the boundary layer thickness, δ , and the time scale, t_s , required for a grain to escape from a wave induced vortex. Although the quantitative procedures for predicting C_o , E_b , and E_s are straightforward, they are much too lengthy for presentation here. They can be found in Nielsen and Green (in press).

The important point here is that observed concentration profiles from Cable Beach showed very close fit to values predicted by equation 18 for breaking waves or equation 19 for unbroken waves and are consistent with laboratory and other field data. Figure 13 shows a concentration profile as predicted by equation 18 together with actual concentration values observed under spilling breakers over the low-tidal zone at low tide. Runs made seaward of the break showed similar fit to equation 19. Although scatter was slightly greater than indicated in Figure 13 in some cases, close fit was observed in all cases. These results suggest that, despite the presence of tidal and other currents, sediment entrainment and suspension was probably due largely to waves.

Once placed in suspension by waves, sediments should be advected by the net currents which, over the subtidal and low-tidal zones were primarily tidal currents with a velocity asymmetry toward the north. Since Cable Beach faces directly into the dominant waves and since oblique wave approach was not observed during the experiments, tidal currents are probably the major cause of longshore transport. Quite simply, the major process of longshore transport is probably as follows: shore-normal waves suspend sediments and asymmetric tidal currents
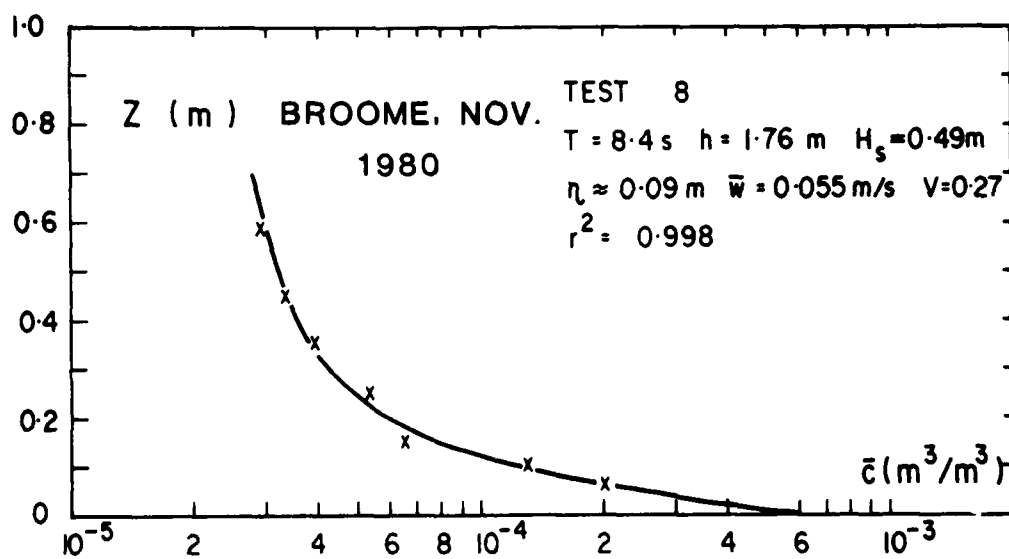
Figure 13. Observed (x) and modelled (solid line; eq. 18) values of suspended
            sediment concentration at different elevations under gently spilling
            breakers over the low-tidal zone.

transport the sediments from south to north. Patterns of sediment accumulation, inlet fill, and spit recurvature to the north of the field site are strongly indicative of a northerly "littoral drift".

Beach Mobility and Temporal Changes

Figure 14 shows the total range of variation, variance of day-to-day elevation, and net change over the survey period of sand level at different points on the intertidal profile based on daily surveys as well as the maximum and average depths of disturbance which occurred between surveys. The net change in profile configuration over the 19-day survey period was negligible, suggesting that the profile was probably in long-term equilibrium with the conditions which prevailed over this period. Changes on a day-to-day basis (as expressed by the square root of the variance curve) were more significant and probably reflected changes in tidal range over the lunar cycle as well as some comparatively minor day-to-day fluctuations in wave height. From the variance and absolute (total) change in elevation curves (Fig. 14), it is apparent that the greatest mobility occurred in the vicinity of the ridge on the high-tidal zone and on the upper part of the mid-tidal zone. Seaward of the upper mid-tidal zone, mobility decreased progressively, consistent with the observations of Short (1981) and Wright (1981) that highly dissipative beach states (i.e. the low-tidal zone, Fig. 9) are the least mobile. Mobility also decreased rapidly to zero at the back of the high tidal beach due to the low frequency of inundation of that part of the beach. The region of maximum mobility on the high-tidal and upper low-tidal zone corresponds to the position of the coarsest material (Fig. 5), high f_w and the associated secondary maximum of time-averaged work rate (Fig. 7). It is also worth noting that the beach state in this region, as indexed by ε (Fig. 9) was intermediate between the reflective and dissipative
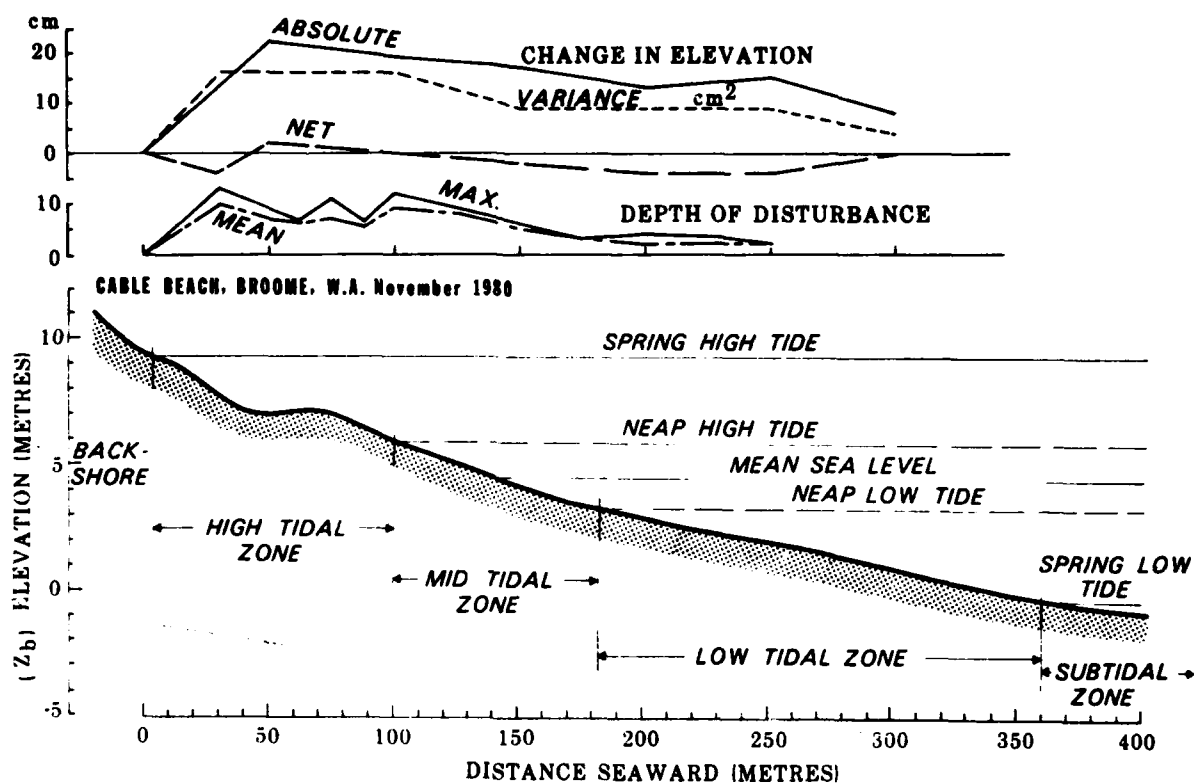
Figure 14. Beach mobility across the intertidal profile expressed in terms of
changes in local sand elevation and depth of disturbance. The
variance of day-to-day sand surface elevation is shown by the dashed
curve. The solid "absolute change in elevation" curve shows the
maximum range of change observed over the study period (maximum Z_b
minus minimum Z_b). The net change curve indicates the accretion
(positive change) or erosion (negative change) over the study period.
The depth of disturbance curves show the mean and maximum depths to
which the bed was scoured beneath subsequently redeposited sand
within individual tidal cycles.

extremes. This mobility was manifest in part by a slight shoreward migration of the ridge.

The depth of disturbance curve in Figure 14 indicates the maximum vertical thickness of the sand layer eroded and subsequently redeposited within a tidal cycle. It is an expression of the migration across the intertidal beach of alternate regions of scour and deposition, probably in a manner similar to that described by Strahler (1964). In most localities, the average depth of disturbance exceeded the standard deviation of sand level suggesting greater variation within tidal cycles than between cycles. The region of maximum depth of disturbance roughly coincided with the region of maximum variance in sand level. An important geological consequence of the tidal cycle alternations of local "cut and fill" is to produce alternating coarse and fine laminae within the beach matrix.

Conclusions

Cable Beach is distinguished from other beaches by the large tidal range which it experiences. If temporal constancy of morphology in the presence of a comparatively stationary set of dynamic forces can be considered an index of short-term morphodynamic equilibrium, then Cable Beach, as we observed it, may be considered a reasonable approximation to the equilibrium state of macrotidal beaches in low to moderate wave energy environments. The processes which operate to achieve and maintain this state on Cable Beach may be assumed to be roughly analogous to those which operate on other macrotidal beaches.

Cable Beach is similar to beaches in low tide range environments in one important respect: wind-generated waves and swell perform most of the work over the entire subtidal and intertidal profile and are primarily responsible for the entrainment and suspension of sediment. However, the morphology of microtidal

beaches is molded largely by surf zone and swash processes. On macrotidal beaches like Cable Beach this is true only of the high tidal zone and in that zone these processes operate only intermittently with active periods separated by long periods of inactivity. Dynamically, the mid-tidal, low-tidal and subtidal zones are probably more similar to the nearshore/offshore zones fronting microtidal beaches. The dominance of these zones by shoaling unbroken waves and, to a lesser degree, by tidal currents suggests that their equilibrium condition should be defined in terms of those processes rather than in terms of surf zone processes.

Surf zone processes are significantly modulated by the constantly changing tidal elevations. The back-and-forth sweep of the surf zone across the concave-upward profile causes continual variations in surf zone and swash zone bed gradient, in breaker conditions and in reflectivity. An important consequence of this is to suppress the growth of resonant phenomena such as edge waves. It is possibly for this reason that no significant rip cells or longshore topographic rhythmicities were observed. On Cable Beach, it was tidal currents rather than wave-induced rips or longshore currents that dominated the net circulation.

At the time of our study, temporal variations in local dynamic regime were more a consequence of the continual variation in local depth than of day-to-day changes in wave energy. Conceptually, these constant changes would be expected to sustain a degree of instantaneous disequilibrium and thereby cause mobility. From the depth of disturbance, bed elevation variance, and net change data, the greatest mobility was observed on the shortest time scale; that is, within individual tidal cycles. The least mobility and nearest approximation to a "steady state" occurred at the longer time scale of the lunar month.

Acknowledgements

References

Boon, J.D. and Byrne, R.J., 1981. "On basin hypsometry and the morphodynamic response of coastal inlet systems". Mar. Geol., v. 40, pp. 27-48.

Bradshaw, M.P., Chappell, J., Hales, R.S. and Wright, L.D., 1978. "Field monitoring and analysis of beach and inshore hydrodynamics". Proc. Aust. Coastal and Ocean Engineering Conf., 4th (Adelaide), pp. 171-175.

Coleman, J.M. and Wright, L.D., 1978. "Sedimentation in an arid macrotidal alluvial river system: Ord River, Western Australia". J. Geol., v. 86, pp. 621-642.

Davis, R.A., Fox, W.T., Hayes, M.O. and Boothroyd, J.C., 1972. "Comparison of ridge and runnel systems in tidal and non-tidal environments". J. Sed. Petrology, v. 42, pp. 413-421.

Fujinawa, Y., 1979. "Some properties of surf beats". Journal of the oceanographical Society of Japan, v. 35, pp. 9-25.

Gresswell, R.K., 1937. "The geomorphology of the south-west Lancashire coastline". Geog. Jour., v. 90, pp. 335-348.

Guza, R.T. and Davis, R.E., 1974. "Excitation of edge waves by waves incident on beach". J. Geophys. Res., 79(9):1285-1291.

Guza, R.T. and Inman, D.L., 1975. "Edge waves and beach cusps". J. Geophys. Res., 80(21):2997-3012.

Holman, R.A., 1981. "Infragravity energy in the surf zone". J. Geophys. Res., v. 86, pp. 6442-6450.

Huntiey, D.A., 1978. "Long period waves on a natural beach". J. Geophys. Res., v. 81, pp. 6441-6449.

Huntley, D.A. and Bowen, A.J., 1975a. "Comparison of the hydrodynamics of steep and shallow beaches". In: J.R. Hails and A. Carr (editors), Nearshore

Sediment Dynamics and Sedimentation, Wiley, New York, N.Y., 316 pp.

Huntley, D.A. and Bowen, A.J., 1975b. "Field observations of edge waves and their effect on beach material". J. Geol. Soc., London, v. 131, pp. 69-81.

Huntley, D.A., Guza, R.T. and Thornton, E.B., 1981. "Field observations of surf beat 1: Progressive edge waves". J. Geophys. Res., v. 86, pp. 6451-6466.

Jonsson, I.G., 1967. "Wave boundary layers and friction factors". Proc. Int. Conf. Coastal Eng., 10th (Tokyo, 1966), Chapt. 10.

King, C.A.M., 1972. Beaches and Coasts (2nd ed.), London, Macmillan, 570 p.

King, C.A.M. and Barnes, F.A., 1964. "Changes in the configuration of the intertidal beach zone of part of the Lincolnshire Coast since 1951". Zeits. fur Geomorph., NF 8, pp. 105-126.

Komar, P.D., 1978. "Relative quantities of suspension versus bedload transport on beaches". J. Sediment. Petrol., v. 48, pp. 921-932.

Nielsen, P., 1979. Some basic concepts of wave sediment transport. Institute of Hydrodynamics and Hydraulic Engineering, Technical University of Denmark, Series Paper 20, Lyngby.

Nielsen, P., 1981. "Dynamics and geometry of wave-generated ripples". J. Geophys. Res., v. 86, pp. 6467-6472.

Nielsen, P. and Cowell, P.J., 1981. Calibration and data correction procedures for flow meters and pressure transducers used by the coastal studies unit. Coastal Studies Unit, Tech. Rept. 811, Coastal Studies Unit, University of Sydney, 33 p.

Nielsen, P. and Green, M.O., in press. "Suspended sediment under waves". Jour. Waterways, Harbours, and Coastal Engineering Div., Am. Soc. Civ. Eng.

Pingree, R.D. and Griffiths, D.K., 1979. "Sand transport paths around the British Isles resulting from M_2 and M_4 tidal interactions". J. Mar. Biol.: Assoc. U.K., v. 59, pp. 467-513.

Price, W.A., 1963. "Patterns of flow and channeling in tidal inlets". <u>J. Sed</u>. <u>Petrol</u>., v. 33, pp. 279-290.

Semeniuk, V., 1981. "Long-term erosion of the tidal flats, King Sound, North Western Australia". <u>Marine Geology</u>, v. 43, pp. 21-48.

Seymour, R.J., 1980. "Longshore sediment transport by tidal currents". <u>J. Geo-phys. Res</u>., v. 85, pp. 1899-1904.

Short, A.D., 1979a. "Wave power and beach stages: A global model". <u>Proc. Int. Conf. Coastal Eng</u>., 16th, pp. 1145-1162.

Short, A.D., 1979b. "Three dimensional beach stage model". <u>J. Geol</u>., v. 87, pp. 553-571.

Short, A.D., 1980. "Beach response to variations in breaker height". <u>Proc. Int. Conf. Coastal Eng</u>., 17th, Sydney.

Short, A.D. and Wright, L.D., 1981. "Beach systems of the Sydney Region". <u>Aust. Geog</u>., v. 15, pp. 8-16.

Sonu, C.J., Pettigrew, N. and Fredericks, R.G., 1974. "Measurements of swash profile and orbital motion on the beach". In: Ocean Wave Measurement and Analysis. Am. Soc. Civ. Eng., v. 1, pp. 621-638.

Strahler, A.N., 1966. "Tidal cycle of changes on an equilibrium beach". <u>J. Geol</u>., v. 74, pp. 247-268.

Swart, D.H., 1974. "Offshore sediment transport and equilibrium beach profiles". Delft Hydraulics Laboratory, Publ. No. 131, Delft, Netherlands.

Thom, B.G., Wright, L.D. and Coleman, J.M., 1975. "Mangrove ecology and estuarine geomorphology: Cambridge Gulf-Ord River, Western Australia". <u>Jour. Ecology</u>, v. 63, pp. 203-232.

Watts, G.M. and Dearduff, R.F., 1954. "Laboratory study of the effect of tidal action on wave-formed beach profiles". U.S. Army Corps of Engineers, <u>Beach Erosion Board Tech. Memo 52</u>, 21 p.

Wright, L.D., 1981. "Modes of beach cut in relation to surf-zone morphodynamics".

    Proc. Int. Conf. Coastal Eng., 17th, Sydney, 1980.

Wright, L.D., in press. "Field observations of long-period surf-zone standing

    waves in relation to contrasting beach morphologies". Aust. J. Mar.

    Freshwater Res.

Wright, L.D., Chappell, J., Thom, B.G., Bradshaw, M.P. and Cowell, P., 1979a.

    "Morphodynamics of reflective and dissipative beach and inshore systems:

    Southeastern Australia". Mar. Geol., v. 32, pp. 105-140.

Wright, L.D., Thom, B.G., and Chappell, J., 1979b. "Morphodynamic variability

    of high energy beaches". Proc. Int. Conf. Coastal Eng., 16th, pp. 1180-1194.

Wright, L.D., Guza, R.T. and Short, A.D., 1981. "Dynamics of a high-energy

    dissipative surf zone". Mar. Geol., v. 43, pp.

Figure Captions

Figure 1. Location map of the study site. The main experiment site was centered on profile M-4. The location of the self-contained underwater data logging/current metering system is indicated by the initials D.L.

Figure 2. Tidal elevations at Broome over the study period, 11-31 November 1980. The zero position corresponds to mean spring low water. The horizontal bars indicate the times and durations of experimental runs.

Figure 3. Instrument locations and tidal levels associated with different experimental runs.

Figure 4. General profile of the subtidal, intertidal, and backshore zones of Cable Beach (profile M-4; based on survey of 12-14 November 1980).

Figure 5. Morphologic details of the subtidal and intertidal profiles, definitions of intertidal zones, variation in grain diameter, and relative frequency of inundation over the profile (profile M-4).

Figure 6. Subtidal dissipation of energy flux, P , as a function of tidal elevation, η_t , and deep water wave height, H_∞ . The loss of energy flux, ΔP , is expressed as a fraction of the total deep water energy flux, P_∞ .

Figure 7. Average energy flux dissipation rates $(dP/dx)_t$ over the lunar half cycle as computed from equation 15 for different wave heights, H_o . The solid curves show the distribution computed on the basis of the actual local friction factors f_w for the rippled bed. The associated f_w values are indicated on the profile. The dashed curves show the hypothetical dissipation rates for a smooth, unrippled bed.

Figure 8. Time-averaged (lunar half cycle) surf-zone dissipation rate $(dP/dx)_s$ relative to the total (surf zone plus non-breaking) dissipation rate

$(dP/dx)_t$. When the curve lies below the 0.5 level, the implication
is that more work is performed by non-breaking shoaling waves than by
surf zone processes.

Figure 9. Variation across the intertidal profile of the surf-scaling parameter,
ε , computed for 12-second incident waves of different heights.

Figure 10. Power spectra, coherence, and phase of surface elevation η (pressure)
and shore normal current, μ measured over the mid-tidal $(x = 100$ m)
and high-tidal $(x = 50$ m) zones.

Figure 11. Shore-parallel current velocity, v , as recorded over the subtidal
zone from a depth of -8 metres below mean water level and corre-
sponding tidal elevations, η_t .

Figure 12. Relative speeds of significant wave orbital velocities, u_s , infra-
gravity oscillations u_{in} and v_{in} , net shore normal flows, $\bar{u}$, and
shore parallel tidal currents, v_t , over the subtidal, low-tidal,
mid-tidal, and high-tidal zones. Values are all shown as non-
dimensional ratios of the local average values of u_s which are
assigned values of 1.

Figure 13. Observed (x) and modelled (solid line; eq. 18) values of suspended
sediment concentration at different elevations under gently spilling
breakers over the low-tidal zone.

Figure 14. Beach mobility across the intertidal profile expressed in terms of
changes in local sand elevation and depth of disturbance. The
variance of day-to-day sand surface elevation is shown by the dashed
curve. The solid "absolute change in elevation" curve shows the
maximum range of change observed over the study period (maximum Z_b
minus minimum Z_b). The net change curve indicates the accretion

(positive change) or erosion (negative change) over the study period. The depth of disturbance curves show the mean and maximum depths to which the bed was scoured beneath subsequently redeposited sand within individual tidal cycles.

APPENDIX 1

The quantities H_5 and U_0 were computed from the total variance, σ^2 in the wind wave band (3 to 30 seconds) from

$$H_5 = 4\sigma$$

and

$$U_5 = 2\sigma$$

The root means square wave height, Hrms is defined on the basis of the variance as

$$Hrms = 2\sqrt{2\sigma^2} = 2\sqrt{2}\ \sigma$$

Hence H_5 and Hrms are related by

$$\frac{H_5}{Hrms} = \sqrt{2}$$

Conventional formula for energy density E are expressed for monochromain waves of wave height H which is equivalent to Hrms by

$$E = \tfrac{1}{8}\ PgH^2$$

However since we wish to estimate average E on the basis of H_5 we must use

$$E = \tfrac{1}{8}\ Pg(H_5/\sqrt{2})^2 = \tfrac{1}{16}\ PgH_5^2$$

Reference: Longuet-Higgins, M.S. 9152 "on the statistical distribution of the heights of sea waves". <u>Journ. of Mar. Res.</u> v. 11 pp. 245-266.

REPORT DOCUMENTATION PAGE		READ INSTRUCTIONS BEFORE COMPLETING FO
1. REPORT NUMBER	2. GOVT ACCESSION NO. AD A114 064	3. RECIPIENT'S CATALOG NUMBER
4. TITLE (and Subtitle) MORPHODYNAMICS OF A MACROTIDAL BEACH: BROOME, WESTERN AUSTRALIA		5. TYPE OF REPORT & PERIOD COVERED TECHNICAL REPORT
		6. PERFORMING ORG. REPORT NUMBER TECHNICAL REPT 82/1
7. AUTHOR(s) L.D. WRIGHT, P. NIELSEN, A.D. SHORT & M.O. GREEN		8. CONTRACT OR GRANT NUMBER(s) GRANT N-00014-80-G-0001
9. PERFORMING ORGANIZATION NAME AND ADDRESS UNIVERSITY OF SYDNEY COASTAL STUDIES UNIT SYDNEY, NSW, 2006, AUSTRALIA		10. PROGRAM ELEMENT, PROJECT, TASK AREA & WORK UNIT NUMBERS NR 388-157
11. CONTROLLING OFFICE NAME AND ADDRESS Office of Naval Research Coastal Sciences Programs, Code 422CS Arlington, VA, 22217, U.S.A.		12. REPORT DATE JANUARY 1982
		13. NUMBER OF PAGES
14. MONITORING AGENCY NAME & ADDRESS(if different from Controlling Office)		15. SECURITY CLASS. (of this report) UNCLASSIFIED
		15a. DECLASSIFICATION/DOWNGRADING SCHEDULE

16. DISTRIBUTION STATEMENT (of this Report)

DISTRIBUTION OF THIS DOCUMENT IS UNLIMITED

17. DISTRIBUTION STATEMENT (of the abstract entered in Block 20, if different from Report)

18. SUPPLEMENTARY NOTES

19. KEY WORDS (Continue on reverse side if necessary and identify by block number)

BEACHES, SURFZONES, MORPHODYNAMICS, MACROTIDAL

20. ABSTRACT (Continue on reverse side if necessary and identify by block number)

An intense field investigation of hydrodynamic processes, processes of sediment entrainment and suspension, and morphologic change was carried out on an unprotected macrotidal beach near Broome in Northwestern Australia. The spring tide range was 9.5 metres; waves had heights of 0.5 to 1.2 metres and periods of 9 to 13 seconds. The beach had an overall concave upward profile with low gradient and dissipative subtidal and low-tidal zones, and steeper more reflective mid-tidal and high-tidal zones. Direct measurement of energy flux dissipa-

tion over the intertidal profile showed dissipation rates on the order of 2 to 5 watts per square metre of bed and indicated an approximate balance between shoaling and dissipation of unbroken waves so as to maintain a constant wave height. Time-averaged predictive estimates of wave work over the lunar half cycle for different points on the intertidal profile show similar dissipation rates and reveal a relatively uniform distribution of work over most of the profile but with maxima in the middle of the low-tidal zone and over the lower part of the high-tidal zone. Most of the work over the low-tidal and mid-tidal zones was performed by unbroken shoaling waves rather than by surf-zone processes; surf zone processes only dominate over a high-tidal zone. The nature of the surf zone processes varied across the profile as local gradient and degree of reflectivity changed with changing tide level. The growth of standing waves and infragravity ("surf beat") oscillations, as indicated from spectra and cross spectra of surface elevation, η, and currents, u and v, was inhibited over most of the profile. However, well developed secondary standing wave energy, particularly at infragravity frequencies, was observed over a high tide. Over the low-tidal and subtidal zones, strong shore-parallel tidal currents were subordinate only to the orbital velocities of unbroken incident waves. Over the subtidal zone asymmetrical tidal currents, skewed toward the north, attained maximum speeds of 0.5 m sec^{-1} just after high water. Field measurements of suspended sediment concentration profiles under broken and unbroken waves showed very good fit to a diffusion model for wave-induced sediment suspension and suggested that sediment suspension was probably attributable largely to waves. Northerly advection of wave-suspended sediment by asymmetrical tidal currents over the subtidal and low-tidal zones accounted for a net northerly longshore transport. The greatest morphological mobility of the intertidal profile occurred over the lower high-tidal and upper mid-tidal zones corresponding to the position of the coarsest material and secondary maximum of time averaged wave work and to a beach state intermediate between the reflective and dissipative extremes. Temporally the greatest mobility of the profile as a whole was observed on the short, within-tidal-cycle time scale. Net changes over the longest time scale of a lunar half cycle were negligible.